Dosimetry Techniques and Radiation Test Facilities for Total Ionizing Dose Testing

Federico Ravotti, *Member, IEEE*

***Abstract*— This paper will address dosimetry and monitoring techniques for total ionizing dose (TID) testing of electronics devices. We will first discuss the basic principles of dosimetry, as well as the most common dosimetric quantities and units, used for the determination of the energy deposited in a given medium by ionizing radiation. In Section III, we will give an overview of the available dosimetry techniques for ionizing radiation, along with the basic mechanisms exploited for their operation. In Section IV, we will address issues and factors affecting the dosimetry measurements, as well as we will give some practical "hints" about the selection and use of the presented techniques. Finally, a synthesis of the existing radiation test facilities, focusing on the one for TID testing, will be given in Section V. Their interest, limitations, and some practical aspects involving the organization of radiation test campaigns will also be discussed in this paper.**

***Index Terms*— Dosimetry, ionizing radiation sensors, radiation effects, test facilities, total ionizing dose (TID).**

I. Introduction

CUMULATIVE radiation effects are gradual effects taking place during the whole lifetime of the electronic component exposed in a radiation environment. Ionizing radiation generates electron–hole (e–h) pairs in insulators, such as the gate, field and spacer oxides (SiO_2) used in integrated circuits (ICs) that can lead to components degradation or failure via total ionizing dose (TID) [1]. An electronic device sensitive to TID will thus exhibit failure in a radiation environment when the accumulated TID reaches its tolerance limit [2]. Therefore, in principle, by setting-up dedicated radiation test campaigns it is possible to predict when a failure will happen for a given, well-known, and characterized electronic component.

Radiation sources typically used for TID testing are Cobalt-60 (^{60}Co) and Cesium-137 (^{137}Cs) radioisotopes (mounted in pool, pop-up sources, or fully shielded irradiators) and low-energy (approximately 10-keV photons) X-ray generators [3].

Radioisotopes are high-energy photon sources that are mainly used for device characterization. Low-energy X-ray generators are instead commonly employed for transistors characterization because of their relatively low cost, the possibility to reach elevated doses within short testing time, their wide distribution worldwide, and their high safety standards (provided that care is taken in the accurate administration of the dose, as explained in Section IV). Moreover, because TID effects often occur in conjunction with single-event effects (SEEs) and displacement damage (DD), it is important to understand the mechanisms responsible for TID in those cases where, for example, both SEE and TID need to be measured [4]. This can be achieved simultaneously using proton beams [5]. Finally, to reach a high TID level, electron beams can also be used as a source of ionization, provided that their energy is kept low enough not to produce DD in the semiconductor material [2]. However, due to the low penetration of electrons this is not favored as a test method. On the other hand, the radiation from accelerator-based sources such as the electron beam can be controlled making the operation of these sources flexible and more secure [6].

Standardized test procedures, such as the ESCC 22900 Iss.5 (2016) [7] or the MIL-STD-883 TM 1019.9 [8], define that the radiation impinging on the tested device must be characterized ideally in terms of radiation energy, spectrum, and dose rate. Precise and accurate dosimetry measurements during TID testing are thus a fundamental ingredient to enable reliable predictions for radiation hardness assurance in nuclear, space [9], high energy physics (HEP) [10], as well as in other applications of electronic systems.

In this paper, we focus on dosimetry techniques for electromagnetic radiation (X-ray, γ-ray, and electrons) and proton particle beams. In Section II, the basic principles of dosimetry are discussed as well as some equations and tools for TID calculations are presented. In Section III, an overview of the most commonly used dosimeters for ionizing radiation is given, along with the basic mechanisms exploited for their operation. Section IV describes the common issues affecting dosimetric measurements and gives practical "hints" for TID measurements during electronics testing. Finally, an overview of the available irradiation facilities and some best practices in TID radiation testing are given in Section V.

Mechanisms of interaction of radiation with matter will not be treated in this paper, as well as the dosimetry quantities recalled here refers to the monoenergetic case only, unless specified otherwise.

II. Dosimetric Principles, Quantities and Units

A. Basic Principles

The activity (A) of an amount of radioactive nuclide (radioisotope) in a particular energy state at a given time is defined as the quotient of dN by dt, where dN is the

Manuscript received January 27, 2018; revised April 15, 2018; accepted April 15, 2018. Date of publication April 25, 2018; date of current version August 15, 2018. This work was supported by the European Union's Horizon 2020 research and innovation program under Grant 654168.

The author is with the Experimental Physics Department, CERN, CH-1211 Geneva, Switzerland (e-mail: federico.ravotti@cern.ch).

Color versions of one or more of the figures in this paper are available online at http://ieeexplore.ieee.org.

Digital Object Identifier 10.1109/TNS.2018.2829864

expectation value of the number of spontaneous nuclear transitions from that energy state in the time interval dt [11]

$$A = dN/dt \quad [\text{Bq}]. \tag{1}$$

The name for the unit of activity is the Becquerel (Bq), where 1 Bq is equal to 1 transition (or disintegration) per second (s^{-1}). The former unit of activity was the Curie (Ci), where 1 Ci $= 3.7 \times 10^{10}$ Bq. The "particular energy state" is the ground state of the nuclide unless specified otherwise. The activity is also equal to the product of the decay constant (λ) for that state and the number of nuclei in that state (N), which is

$$A = N \times \lambda \quad [\text{Bq}]. \tag{2}$$

The decay constant λ of a radioactive nuclide in a particular energy state is the quotient of dP by dt, where dP is the probability of a given nucleus undergoing a spontaneous nuclear transition from that energy state in the time interval dt. The quantity $T_{1/2} = \ln(2)/\lambda = 0.693/\lambda$ is commonly referred as the half-life of the radioactive nuclide, that is, the time taken for the activity of an amount of radioactive nuclide to become half its initial value.

Ionization is the process by which an atom or a molecule acquires a negative or positive charge by gaining or losing electrons to form an ion pair, often in conjunction with other chemical changes. Ionization can result from the "direct" loss of an electron after collisions with charged particles (electrons, protons, etc.), other atoms, molecules, and ions, or "indirectly" through the interaction with X- or γ-photons and neutrons. A detailed treatment of the mechanisms of energy transfer from radiation to matter is given in [12].

Radiation dosimetry deals with methods for a quantitative determination of energy deposited in a given medium by directly or indirectly ionizing radiations. A number of quantities and units have been defined for describing the radiation field at the point of interest. This section describes the most commonly used dosimetric quantities for ionizing radiations and their units, based on the excellent summary of this topic given in the IAEA publication by Podgorsak [13]. A very simplified discussion of the theory that deals with calculating the response of a dosimeter in a medium (cavity theory) is given in Section II-F and has been adapted here from [1] and tutorial lectures given in [14].

B. Photon and Particle Fluence

The following quantities are used to describe a monoenergetic ionizing radiation beam: particle fluence, energy fluence, particle fluence rate, and energy fluence rate. These are used to describe both photon (Section II-E1), electrons (Section II-E2), and charged particle beams (Section II-E4).

The particle fluence Φ is the quotient dN by dA, where dN is the number of particles incident on a sphere of cross-sectional area dA

$$\Phi = dN/dA \quad [\text{cm}^{-2}]. \tag{3}$$

The unit of particle fluence is typically cm^{-2}. The use of a sphere of cross-sectional area dA expresses the fact that one considers an area dA perpendicular to the direction of each particle, and hence that particle fluence is independent of the incident angle of the radiation.

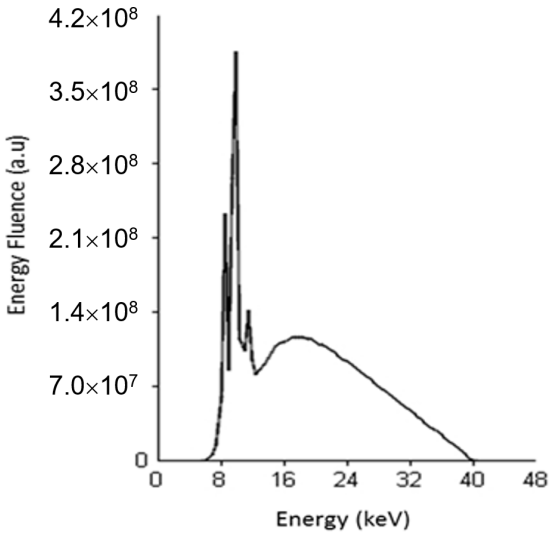

Fig. 1. Energy fluence spectrum at 1 m from the W target of an X-ray tube with a potential of 40 kV and added filtration of 0.15-mm Al and 0.25-mm Be. The characteristic peak emission of the W target (L line) is also visible here.

The energy fluence Ψ is the quotient of dE by dA, where dE is the radiant energy incident on a sphere of cross-sectional area dA

$$\Psi = dE/dA \quad [\text{J/cm}^2]. \tag{4}$$

The unit of energy fluence is J/cm^2. For monoenergetic radiation, the energy fluence can be calculated from particle fluence (3) by using the following relation:

$$\Psi = \frac{dN}{dA}E = \Phi E. \tag{5}$$

In (5), E is the energy of the ionizing radiation and dN represents the number of photons or particles with energy E.

Almost all realistic photon or particle beams are polyenergetic and the above-defined concepts need to be applied to such beams, namely, the particle fluence spectrum (6) and energy fluence spectrum (7) replace the particle fluence (3) and energy fluence (4), respectively

$$\Phi_E(E) = \frac{d\Phi}{dE}(E) \tag{6}$$

$$\Psi_E(E) = \frac{d\Phi}{dE}(E)E. \tag{7}$$

An example of polyenergetic spectrum is given in Fig. 1, which shows the energy fluence spectrum generated by an X-ray tube available at European Organization for Nuclear Research (CERN), Geneva, Switzerland with a peak value (kV_p) of 40 kV, target material tungsten (W), and an added filtration of 0.15 mm of aluminum (Al), and 0.25 mm of beryllium (Be) [15]. The spikes superimposed on the continuous bremsstrahlung spectrum represent the characteristic X-ray lines produced in the W target (Section V-B).

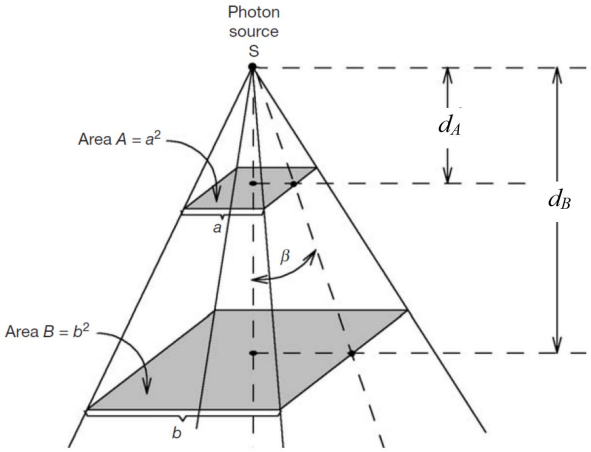

Fig. 2. Divergent photon beam originating in a photon point source. Adapted from [13].

The particle fluence rate is the quotient of $d\Phi$ by dt, where $d\Phi$ is the increment of the fluence in time interval dt

$$\dot{\Phi} = d\Phi/dt \quad [\mathrm{cm}^{-2} \cdot \mathrm{s}^{1}]. \tag{8}$$

By analogy, the energy fluence rate $\dot{\Psi}$ is instead the quotient of $d\Psi$ by dt, where $d\Psi$ is the increment of the energy fluence in the time interval dt. The typical unit of energy fluence rate is J/(cm$^2 \cdot$ s).

C. Photon Source Geometry and Beam Attenuation

Photon sources for TID testing are either isotropic or nonisotropic, and they emit either monoenergetic (radioisotopes) or polyenergetic (X-ray tubes) photon beams.

An isotropic photon source produces the same photon fluence rate in all directions, while the photon fluence rate from a nonisotropic source depends on the direction of measurement.

In most practical situations, photon sources can often assumed to be a point source and the beams they produce are divergent beams, as shown in Fig. 2.

Let us now consider a point source S and a square field (spherical segment) with side a (area $A = a^2$) at a distance d_A from the source. At a distance d_B there will be a square field with side b (area $B = b^2$). If the source S emits photons and produces a fluence Φ_A at d_A and a fluence Φ_B at d_B, since the total number of photons crossing the two areas must be constant, it is possible to demonstrate that for equivalent solid angles [13]

$$\frac{\Phi_A}{\Phi_B} = \frac{d_B^2}{d_A^2}. \tag{9}$$

The photon fluence is thus inversely proportional to the square of the distance from the source. For example, if $d_B = 2d_A$ then the photon fluence at B will be exactly 1/4 of the photon fluence at A. Since the Kerma in air and the "dose to small mass of medium in air" (Section II-E1) are directly proportional to the photon fluence, it is reasonable to conclude that all the quantities defined later on follow this inverse square law behavior.

Photons undergo various possible interactions with the atoms of the material they cross, acting as an attenuator; the probability or cross section for each interaction depends on the energy $E = h\nu$ of the photon and on the atomic number Z of the attenuator. During the interaction, the photon may completely disappear (photoelectric effect, pair production), or it may be scattered (Compton effect). A detailed description of these phenomena is available in [12] and [16].

The intensity $I(t)$ of a narrow monoenergetic photon beam, crossing an attenuator medium of a thickness t (cm), is thus given as

$$I(t) = I(0) \cdot e^{-\mu \cdot t} \tag{10}$$

where $I(0)$ is the original intensity of the unattenuated beam in terms of the photon fluence and $\mu(\mathrm{cm}^{-2})$ is the linear attenuation coefficient, which depends on the photon energy and attenuator atomic number Z. For use in radiation dosimetry, two additional attenuation coefficients are defined: the energy transfer coefficient (μ_{tr}) and the energy absorption coefficient (μ_{en}) that are related to μ [13] and described later in detail in Section II-E.

D. Kerma, Absorbed Dose and Stopping Power

Kerma is an acronym for kinetic energy released per unit mass. It is a nonstochastic quantity applicable to indirectly ionizing radiations such as photons and neutrons. It quantifies the average amount of energy transferred from indirectly to directly ionizing radiation, without concern as to what happens after this transfer. In the discussion that follows regarding TID, we will focus on photons only. The energy of photons is imparted to matter in a two-stage process. In the first one, the photon radiation transfers energy to the secondary charged particles (electrons) through various photon interactions mentioned earlier [16]. In the second stage, the charged particle transfers energy to the medium through atomic excitations and ionizations.

In this context, the Kerma is defined as the mean energy transferred from the indirectly ionizing radiation to charged particles (electrons) in the medium $d\bar{E}_{\mathrm{tr}}$ per unit mass dm

$$K = d\bar{E}_{\mathrm{tr}}/dm \quad [\mathrm{Gy}]. \tag{11}$$

The unit of Kerma is joule per kilogram. The name for the unit of Kerma is the Gray (Gy), where 1 Gy = 1 J/kg.

Absorbed dose is a nonstochastic quantity applicable to both, indirectly and directly ionizing radiations. For indirectly ionizing radiations, the energy is imparted to matter in two steps. In the first step (resulting in Kerma), the indirectly ionizing radiation transfers energy as kinetic energy to secondary electrons. In the second step, these electrons transfer some of their kinetic energy to the medium by ionization (resulting in absorbed dose) and lose some of their energy in the form of radiative losses (e.g., bremsstrahlung).

The absorbed dose is thus related to the stochastic quantity called energy imparted ε, and is then defined as the mean energy imparted $d\bar{\varepsilon}$ by ionizing radiation to matter of mass dm in a finite volume V of a specified material

$$D = d\bar{\varepsilon}/dm \quad [\mathrm{Gy}]. \tag{12}$$

The mean energy imparted is the sum of the energy entering the volume of interest minus the energy leaving the volume. Since electrons travel in the medium and deposit energy along their tracks, this absorption of energy does not necessarily take place at the same location as the transfer of energy described by Kerma.

The unit of absorbed dose is joule per kilogram. The name for the SI unit of absorbed dose is the Gy. The discontinued unit (but still widely used in the community performing TID testing on electronics) for absorbed dose is the radian 1 rad = 100 erg/g = 0.01 Gy. Since the absorbed dose depends on the material of interest, the specific material should always be specified or referenced in parenthesis directly following the name of the unit: rad(SiO_2), Gy(air), etc. [1].

Stopping powers are widely used in radiation dosimetry, but they are rarely measured and must be calculated from theory. For electrons and positrons, the Bethe theory is used to calculate stopping powers [17]. The (unrestricted) linear stopping power is defined as the expectation value of the rate of energy loss per unit path length (dE/dx) of a charged particle in a medium. The mass stopping power is defined as the linear stopping power divided by the density of the absorbing medium. Division by the density eliminates the dependence of the mass stopping power on mass density. Typical units for the linear and mass stopping powers are MeV/cm and MeV $\cdot$ cm^2/g, respectively.

Two types of stopping power are known: the mass collision (S_{coll}/ρ), resulting from interactions (ionization) of charged particles with atomic orbital electrons, and mass radiative (S_{rad}/ρ), resulting from interactions of charged particles with atomic nuclei. The mass-total stopping power is the sum of the mass-collision and the mass-radiative stopping power [13]. The mass-total stopping power formulas for charged particles (including protons and heavier particles) are given in [18].

The unrestricted mass-collision stopping power expresses the average rate of energy loss by a charged particle in all soft and hard collisions. A soft collision occurs when a charged particle passes an atom at a considerable distance. The net effect of this collision is that a very small amount of energy is transferred to an atom of the absorbing medium. On the contrary, in a hard collision, a secondary electron (often referred to as a δ-electron) with considerable energy is ejected and forms a track.

Fig. 3 depicts the mass-collision stopping power for electrons and protons in some materials of interest for dosimetry [19]. As visible in the plot, S_{coll}/ρ gradually flattens to a broad minimum ($\sim$2 MeV $\cdot$ cm^2/g). A minimum ionizing particle (MIP) is thus a particle with a mean energy loss rate through matter close to the minimum. In many practical cases, relativistic particles are MIPs [18].

The concept of restricted mass-collision stopping power is introduced to calculate the energy transferred to a localized region of interest. By limiting the energy transfer to secondary charged δ-particles to a threshold (denoted by Δ), highly energetic secondary particles are allow escaping the region of interest. The restricted stopping power is lower than the unrestricted stopping power. The choice of the energy threshold depends on the problem to analyze. For problems involving

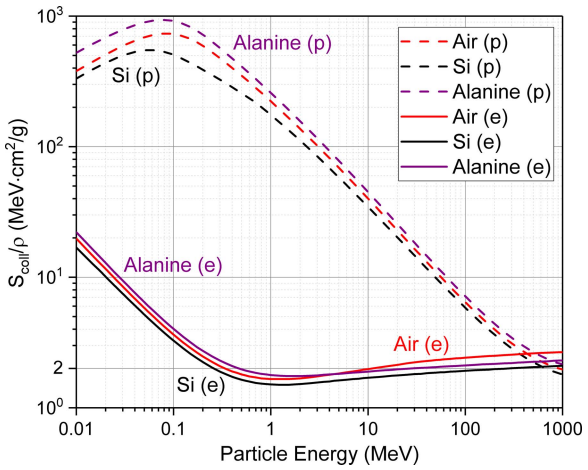

Fig. 3. Mass-collision stopping power for protons and electrons in various materials of interest for dosimetry from [19] and [20].

ionization chambers, for instance, a frequently used threshold value is 10 keV (as explained later, the range of a 10-keV electron in air is $\sim$2 mm).

The restricted linear-collision stopping power LET_Δ (also referred to as restricted linear energy transfer) of a material for charged particles is the quotient of dE_Δ by dl. Where dE_Δ is the energy lost by a charged particle due to soft and hard collisions in traversing a distance dl, minus the total kinetic energy of the charged particles released with kinetic energies in excess of Δ

$$\text{LET}_\Delta = dE_\Delta/dl \quad [\text{keV}/\mu\text{m}]. \tag{13}$$

If Δ tends toward infinity, then there are no electrons with larger energy, and the LET_Δ becomes the unrestricted LET which is identical to the linear stopping power. Being the energy deposed per unit path length, the unit of LET is J/m, often given in keV/μm (1 keV/μm $\approx$ 1.602×10^{-10} J/m). According to this definition, low-LET radiation is X-ray and γ-ray or light charged particles such as electrons that produce sparse ionizing events far apart at atomic scale ($<$10 keV/μm). High-LET radiation is instead heavy charged particles (or neutrons) that produce ionizing events densely spaced at atomic scale ($>$10 keV/μm).

A charged particle such as an electron is surrounded by its Coulomb electric field and will, therefore, interact with one or more electrons or with the nucleus of practically every atom it encounters. Since most of these interactions individually transfer only small fractions of the incident particle's kinetic energy (soft collisions), it is convenient to think of the particle as losing its kinetic energy gradually and continuously in a process often referred to as the continuous-slowing-down approximation (CSDA) [13].

The path length of a single electron is thus the total distance traveled along its actual trajectory until it comes to rest, regardless of its direction of movement. The range (or the mean path length) for an electron is, therefore, a calculated quantity (in the CSDA approximation) that represents the mean path length along its trajectory. The same concept can be extended to all other charged particles. The CSDA range for

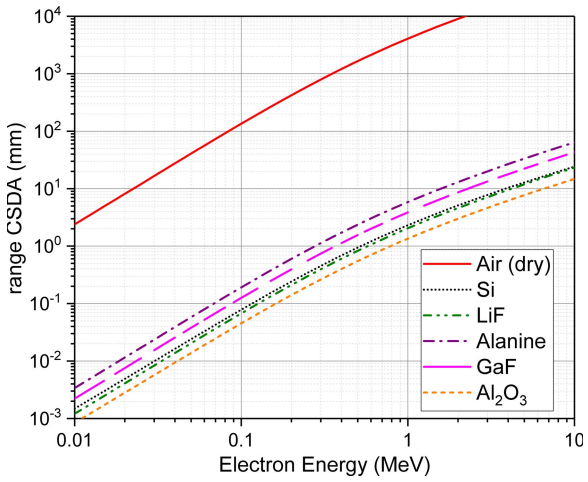

Fig. 4. CSDA ranges for electrons in various dosimetric materials from [19].

electrons in various dosimetric materials is shown in Fig. 4 as a function of the electron energy [20].

E. Relationships Between Various Dosimetric Quantities

1) Energy Fluence and Kerma (Photons): The energy transferred to electrons by photons can be expended in two distinct ways:

1) through (soft and hard) collision interactions;
2) through radiative interactions (bremsstrahlung and electron–positron annihilation).

The total Kerma is, therefore, usually divided into two components: the collision Kerma (K_{coll}) and the radiative Kerma (K_{rad}). The collision Kerma leads to the production of electrons that dissipate their energy as ionization in or near the electron tracks in the medium, and is the result of Coulomb force interactions with atomic electrons. The radiative Kerma leads instead to the production of radiative photons as the secondary charged particles slow down and interact in the medium. The total Kerma (K) is thus given by the following:

$$K = K_{\text{coll}} + K_{\text{rad}}. \tag{14}$$

A frequently used relation between collision Kerma (K_{coll}) and total Kerma (K) may be written by introducing the factor $\bar{g}$ (radiative fraction), representing the average fraction of the energy transferred to electrons that is lost through radiative process. Hence, the fraction lost through collisions is

$$K_{\text{coll}} = K \cdot (1 - \bar{g}). \tag{15}$$

For monoenergetic photons, the collision Kerma at a point in a medium is related to the energy fluence Ψ at that point in the medium by the following relation:

$$K_{\text{coll}} = \Psi \cdot \left(\frac{\mu_{\text{en}}}{\rho}\right) \tag{16}$$

where (μ_{en}/ρ) is the mass–energy absorption coefficient (cm^2/g) for the monoenergetic photons in the medium [21]. For polyenergetic beams, a formally similar relation exists, but it is made of spectrum-averaged quantities [13]. Always for monoenergetic photons, the total Kerma (K) at a point in a medium is related to the energy fluence (Ψ) in the medium by an analogous relation as (16), where the mass–energy transfer coefficient of the medium (μ_{tr}/ρ) for the given photon energy is used instead. If bremsstrahlung production within the specified material is negligible, the mass–energy absorption coefficient is equal to the mass–energy transfer coefficient.

Using (16), one can obtain the relation between collision Kerma in two different materials, $m1$ and $m2$, as follows:

$$\frac{\text{K}_{\text{coll},2}}{\text{K}_{\text{coll},1}} = \frac{\Psi_2 \left(\frac{\mu_{\text{en}}}{\rho}\right)_2}{\Psi_1 \left(\frac{\mu_{\text{en}}}{\rho}\right)_1} = \Psi_{2,1} \left(\frac{\mu_{\text{en}}}{\rho}\right)_{2,1}. \tag{17}$$

Equation (17) is practically used when the fluence ratio $\Psi_{2,1}$ can be assumed to be unity, for example, for similar materials or for situations in which the mass of $m2$ is sufficient to provide buildup (Section II-E3), but at the same time small enough so as not to disturb the photon fluence in $m1$ (e.g., "dose to a small mass of silicon in air").

2) Fluence and Dose (Electrons): Under the conditions that radiative photons escape the volume of interest and secondary electrons are absorbed on the spot (or there is a charged-particle equilibrium (CPE) of secondary electrons—Section II-E3), the absorbed dose to medium D_m is related to the electron fluence Φ_m in the medium as follows:

$$D_m = \Phi_m \cdot \left(\frac{S_{\text{coll}}}{\rho}\right)_m \tag{18}$$

where $(S_{\text{coll}}/\rho)_m$ is the unrestricted mass-collision stopping power of the medium at the energy of the electron. When an electron slows down in a medium, even for a monoenergetic starting electron, there is always present a primary fluence spectrum. In this case, the absorbed dose to the medium can be obtained by integrating (18) over the energy spectrum. Thus, the absorbed dose can be calculated by making use of spectrum-averaged collision stopping power and total fluence. Based on (18) and under the same assumptions used for (17) for two media, $m1$ and $m2$, the ratio of absorbed doses can be calculated as

$$\frac{D_2}{D_1} = \frac{\Phi_2 \left(\frac{S_{\text{coll}}}{\rho}\right)_2}{\Phi_1 \left(\frac{S_{\text{coll}}}{\rho}\right)_1} = \Phi_{2,1} \left(\frac{S_{\text{coll}}}{\rho}\right)_{2,1} \tag{19}$$

where the shorthand notations $\Phi_{2,1}$ and $(S_{\text{coll}}/\rho)_{2,1}$ are being used for the ratio of the electron fluence and the collision stopping powers in the media $m2$ and $m1$, respectively.

3) Kerma and Dose: Charged Particle Equilibrium (CPE): Generally, the transfer of energy (Kerma) from the photon beam to charged particles at a particular location does not lead to the absorption of energy by the medium (absorbed dose) at the same location. This is due to the nonfinite range of the secondary electrons released through photon interactions.

Since radiative photons mostly escape from the volume of interest (as described in Section II-E1), one relates absorbed dose usually to collision Kerma. Thus, the ratio of dose (D) and collision Kerma (K_{coll}) is denoted by

$$\beta = D/K_{\text{coll}}. \tag{20}$$

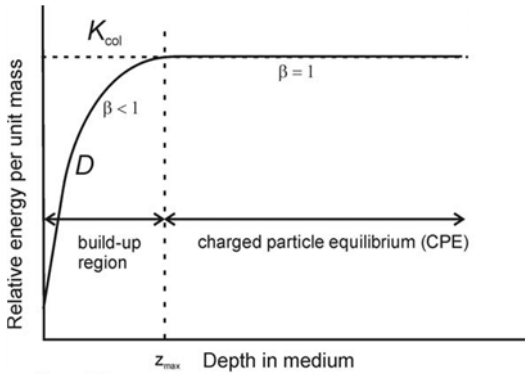

Fig. 5. Collision Kerma and absorbed dose as a function of depth in a medium irradiated by a photon beam for the case of no photon attenuation [13].

If radiative photons escape the volume of interest, an assumption is made that $\beta \approx 1$. Fig. 5 illustrates the relation between collision Kerma and absorbed dose under conditions of CPE.

As a high-energy photon beam penetrates the medium (from the left to the right in Fig. 5), collision Kerma is maximal at the surface of the irradiated material because photon fluence is greatest at the surface. Initially, the charged particle fluence, and hence the absorbed dose, increases as a function of depth until the depth of dose maximum $z_{\max}$ is attained (buildup region). If there were no photon attenuation or scattering in the medium, but yet production of electrons, the buildup region (with $\beta < 1$) would be followed by a region of complete CPE, where $D = K_{\text{coll}}$ (i.e., $\beta = 1$) as illustrated in Fig. 5.

In reality, however, due to photon attenuation and scattering in the medium, a region of transient CPE occurs where, although $\beta > 1$, an essentially constant relation between collision Kerma and absorbed dose exists. This because, the average energy of the secondary electrons generated by high-energy photons, and hence their range, does not change appreciably with depth in the medium. In practice, the thickness of material required to approximate electron equilibrium is equal to the range of the maximum-energy secondary electrons that can be generated by the primary photons (see Fig. 4).

In the special case in which CPE exists (at the depth of maximum dose in the medium, $\beta = 1$), the relation between absorbed dose D and total Kerma K is given by (15), where the radiative fraction $\bar{g}$ has been previously defined. The higher the electrons kinetic energy, the larger is $\bar{g}$. The radiative fraction also depends on the material considered, with higher values of $\bar{g}$ for higher Z materials. As an example, for electrons produced by ^{60}Co rays in air, the radiative fraction equals 0.0032.

Finally, taking into account (5) and (16), under CPE conditions, the absorbed dose for a photon source may be expressed as follows:

$$D = \Phi \cdot E \cdot \left(\frac{\mu_{\text{en}}}{\rho}\right) \tag{21}$$

where Φ and E are the photon fluence and the energy of the ionizing radiation, respectively, and (μ_{en}/ρ) the mass–energy absorption coefficient as defined above.

It is often convenient to refer to a value of Kerma for a specified material in free-space (air) or inside a different material. For measurements of Kerma, the mass element should be so small that its introduction does not disturb much the incident photon field.

4) Fluence and Dose (Charged Particle Beam): The dose to a thin object of a given material placed in a charged particle beam will depend primarily on the rate of energy loss of the particles in that material and their distribution across the beam (Section II-E2). A thin material object is the one with thickness much smaller than the range of the charge particle in the material itself. The TID in Gy from protons and electrons can thus be calculated directly from the mass-collision stopping power and the fluence by extending (18)

$$D = K \times (S_{\text{coll}}/\rho) \times \Phi \quad [Gy] \tag{22}$$

where Φ is the particle fluence expressed in cm^{-2}, $K = 1.602 \times 10^{-10}$ is a scale factor, and the mass-collision stopping power, which has units of MeV·cm^2/g, is obtained from [19] and given here in Fig. 3 for some materials of practical interest. As an example, a 60-MeV proton has a mass-collision stopping power of about 9 MeV $\cdot$ cm^2/g in SiO_2 (LET $\sim$ 2 keV/μm) so that to obtain a TID of 1 kGy in a thin SiO_2 layer of a MOS device will require a fluence of approximately 7×10^{11} p/cm^2, as obtained from (22).

As described in Section II-D, MIPs (e.g., protons with $E > 600$ MeV and muons and pions with $E > 100$ MeV) deposit energy at a rate of about 2 MeV $\cdot$ cm^2/g in practically all target materials. A list of minimum ionizing energy loss rate values for the most common materials is available in [18]. For high-energy charged particles, the contribution of nuclear interactions and the resulting secondaries to the dose in the beam is usually small and so it can be normally neglected [22].

If the material object traversed by the charged particle beam cannot be considered thin, then the above calculation is no longer valid and a full Monte Carlo (MC) simulation may need to be performed (as explained later in Section II-F4).

Although the calculation described above is also valid for evaluating the TID delivered by electron beams of a given energy, one has to be aware that electrons broaden their spectrum when interacting with the accelerator structures and by bremsstrahlung production, as their travel toward the device under test (DUT). All these effects can make accurate dosimetry of electron beams more complex [13] (Section IV-A3).

F. Dose Determination in Semiconductor Materials

1) Practical Considerations: To measure the equilibrium dose in a semiconductor material, for example, silicon (Si), in principle, we should simply surround a small Si detector with an equilibrium thickness of silicon material. The energy absorbed by the small detector, divided by its mass, is the silicon equilibrium dose at the center of this "dosimeter." Now, although this arrangement could possibly be used, it is always difficult to implement in practice.

What is more convenient to do is to surround a passive dosimeter [thermoluminescence dosimetry (TLD), radio-photoluminescence (RPL), etc., in Section III] with an

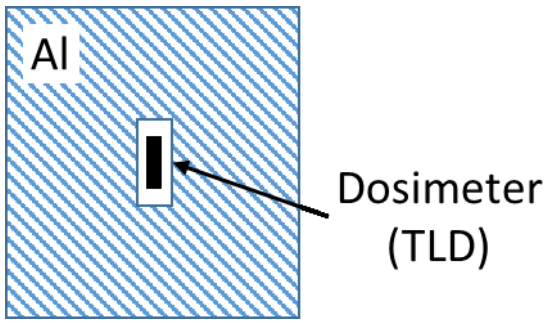

Fig. 6. Example of practical dosimeter configuration: TLD dosimeter inside an Al shield.

equilibrium layer of some material. Typically, neither the dosimeter nor the surrounding equilibrium layer is made of the material of interest (Si). If, for instance, a TLD dosimeter (Section III-D1) shielded with an aluminum (Al) layer is used to measure Si equilibrium dose as shown in Fig. 6, attention must be paid to the energy spectrum of the photon source, as well as in the choice of the materials used. This because the arrangement shown in Fig. 6 represent a Bragg–Gray cavity [23]; in this specific case, a small cavity filled with a TLD dosimeter and surrounded by Al [24], [25].

According to cavity theory, the dose in the wall material (Al) can be immediately related to the measured dose in the detector material (TLD) only in these two limiting cases.

1) If the cavity is much thinner than the range of the secondary electrons produced in the wall material, then (19) applies, where 1 = det, 2 = wall, and $\Phi_{\text{wall,det}} = 1$

$$\frac{D_{\text{wall}}}{D_{\text{det}}} = \left(\frac{S_{\text{coll}}}{\rho}\right)_{\text{wall,det}}. \tag{23}$$

2) If the cavity is much thicker than the range of the most energetic secondary electron produced in the wall material, then CPE is reestablished in the cavity material ($D = K_{\text{coll}}$) and (17) applies where the energy fluence ratio is equal to unity

$$\frac{D_{\text{wall}}}{D_{\text{det}}} = \left(\frac{\mu_{\text{en}}}{\rho}\right)_{\text{wall,det}}. \tag{24}$$

Unfortunately, the cavity dimension is usually somewhere between these two limiting cases and there is no "simple" way to relate D_{wall} with D_{det}. Furthermore, since what is really desired is the equilibrium dose in some other materials of interest (Si), (24) must be used once again to relate D_{Si} with D_{wall}.

Therefore, a dosimeter can be used to measure the equilibrium dose in some reference material only if the two following conditions are both satisfied.

1) The photon source spectrum is known well enough so that all stopping power and absorption coefficient ratios in the previous equations can be calculated.
2) One of the following three conditions applies as well.
   a) One of the two limiting Bragg–Gray cavity cases applies so that the previous equations can be used.
   b) The photon energy spectrum is such that all of the stopping power and absorption coefficient ratios are nearly equal to 1 in the energy region covered by the spectrum of the incident photon radiation (making $D_{\text{Si}} \approx D_{\text{wall}} \approx D_{\text{det}}$).
   c) The dose is calculated using an electron–photon transport calculation tool (Section II-F4).

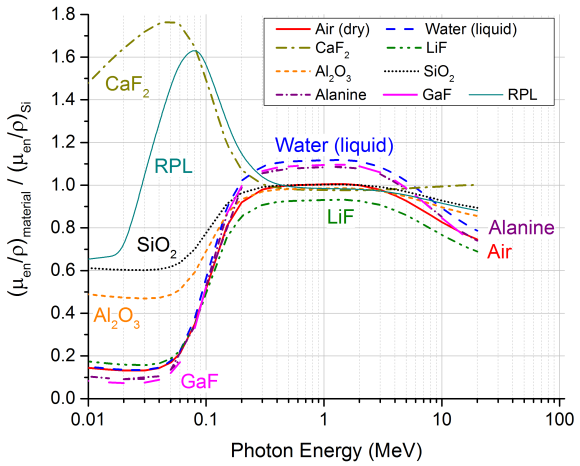

Fig. 7. Ratios of mass-energy absorption coefficients of various dosimetric materials relative to silicon as a function of the photon energy. Data from [21].

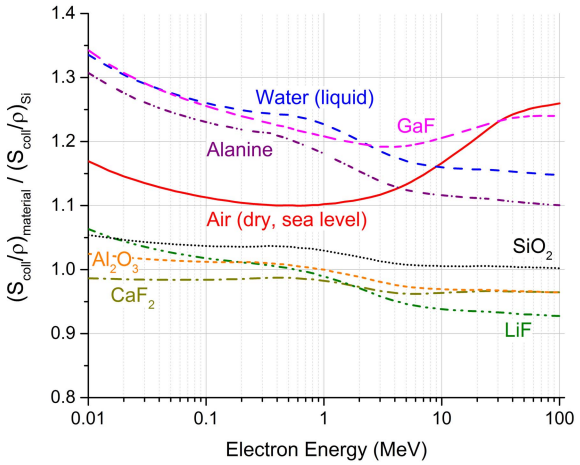

Fig. 8. Ratios of mass-collision stopping powers of various dosimetric materials relative to silicon as a function of the electron energy. Data from [19].

Option 2a is rarely applicable. Option 2c is undesirable, but it is sometimes necessary, especially for sources with photon energy components <200 keV. Option 2b is fortunately applicable for a significant number of cases, namely, those for which the photon energy is mainly above 200 keV and below 10 MeV, and for a wide variety of low-Z materials typically used for dosimetry, as shown in Figs. 7 and 8. By accurately choosing the dosimeter (and equilibrium layer material) for a given practical situation, the errors introduced by this approximation are usually less than about 10%.

The most commonly used dosimeters for TID measurements in radiation hardness testing at radioactive sources, X-ray, and linear accelerator (LINAC) facilities are discussed in Section III.

2) Collision Kerma and Exposure: The exposure (X) is the quotient of dQ by dm, where dQ is the absolute value of the total charge of the ions of one sign produced in air when all

the electrons and positrons liberated or created by photons in the mass dm of air are completely stopped in air

$$X = dQ/dm \quad [\mathrm{C/Kg}]. \tag{25}$$

The unit of exposure is coulomb per kilogram. The unit used for exposure is the Roentgen (R), where 1 $R = 2.58 \times 10^4$ C/kg. In the SI system of units, Roentgen is no longer used.

The average energy expended in air per ion-pair formed is $W_{\mathrm{air}} = 33.97$ eV/ion [13]. Taking this into account and the conversion J/eV, it is possible to demonstrate $W_{\mathrm{air}}/e = 33.97$ J/C.

Therefore, multiplying the collision Kerma by the number of Coulombs of charge created per joule of energy deposited (e/W_{air}) gives the charge created per unit mass of air (e.g., the exposure)

$$X = K_{\mathrm{coll,air}} \times (e/W_{\mathrm{air}}). \tag{26}$$

The relation between total Kerma and exposure is then obtained by combining (15) and (25)

$$K_{\mathrm{air}} = X \times (W_{\mathrm{air}}/e) \times \frac{1}{1-\bar{g}}. \tag{27}$$

Equation (27) shows that air Kerma is the common SI replacement for exposure because these two quantities only differ by a constant factor (0.0087 Gy/R) over a very wide range of photon energies in air, where $\bar{g} \to 0$. The advantage of using the exposure for photon radiation in air is more evident when using the traditional unit rad. Expressing the dose in rad, makes possible to easily convert exposure (X) to dose (D) in air with CPE conditions by applying the appropriate factor: D [rad] = X [R] $\times$ 0.877 [rad/R]. In water or tissue, this constant factor is within the range of 0.94–0.98 (e.g., $\sim$1) for photon energies ranging from 100 keV to 3 MeV. In other materials, other values for this constant apply [26].

3) Gamma Exposure Constants: In practice, it is often necessary to estimate the exposure rate at a distance from radionuclides emitting γ-ray or X-ray. The factor relating activity and exposure in the SI unit, named air Kerma rate constant, is defined as

$$\Gamma_\delta = \frac{l^2}{A}\left(\frac{dK_{\mathrm{air}}}{dt}\right)_\delta \quad [\mathrm{Gy \cdot m^2/(s \cdot Bq)}] \tag{28}$$

where the air Kerma rate in (28) is the one due to photons of energy $> \delta$ at a distance l [m] from a point source of activity A in Bq [27]. The most comprehensive compilation of gamma dose constants is the one published in 1982 by the Oak Ridge National Laboratory, Oak Ridge, TN, USA [28].

4) Calculation Tools: As mentioned earlier for charged particles, or for low-photon energies (Section II-F1), it could be necessary to compute the dose deposed in a given material by photons using MC transport calculation tools. A (nonexhaustive) list of some of the MC codes used for this purpose is given here.

1) *MCNP:* Developed and maintained at Los Alamos, distributed via RSICC (http://rsicc.ornl.gov).
2) *PENELOPE:* Developed and maintained at the University of Barcelona, Barcelona, Spain, distributed via the Nuclear Energy Agency (http://www.nea.fr/abs/html/nea-1525.html).
3) *Geant4:* Developed by a large collaboration in the HEP community (http://geant4.web.cern.ch/geant4/).
4) *EGSnrc:* Developed and maintained at NRC (http://www.irs.inms.nrc.ca/EGSnrc/EGSnrc.html).
5) *FLUKA:* A fully integrated particle physics MC simulation package developed for HEP applications (http://www.fluka.org).
6) *SCALE:* Comprehensive modeling and simulation suite for nuclear safety analysis and design developed and maintained by the Oak Ridge National Laboratory (https://www.ornl.gov/scale).

For protons and ions, the SRIM tools package can also be conveniently used (http://www.srim.org/) [29]. Finally, most of the dosimetry calculations described in this section such as the nuclide decay, photon absorption, or stopping power calculations can be performed with tools available on the web such as NUCLEONICA (https://www.nucleonica.com/) or Rad Toolbox (https://www.ornl.gov/crpk/software). These tools allow obtaining quick results for testing, validating, and verifying complex computer models.

III. Radiation Dosimeters

A radiation dosimeter is a device, instrument or system that measures or evaluates (directly or indirectly) the quantities exposure, Kerma, absorbed dose, or their time derivatives (rates), or related quantities of ionizing radiation. A dosimeter along with its reader is referred to as a dosimetry system.

To function as a radiation dosimeter, the device must have at least one physical property that is a function of the measured dosimetric quantity and that can be properly calibrated. For example, in TID testing, exact knowledge of both absorbed dose to Si or SiO_2 at a specified point, and its spatial distribution, are of importance. The absorbed dose measured by the dosimeter shall be converted to the equilibrium absorbed dose in the material of interest within the critical region of the DUT, for example, the SiO_2 gate oxide of a MOS device [30].

In order to be useful, a radiation dosimeter must exhibit several desirable characteristics which are detailed in Section III-A. Unfortunately, not all dosimeters can satisfy simultaneously all characteristics. Therefore, the choice of a dosimetry system must be made judiciously, taking into account case-by-case requirements.

A. Properties of Dosimeters

1) Accuracy and Precision: In radiation dosimetry, the uncertainty associated with the measurement is often expressed in terms of accuracy and precision.

The precision of dosimetry measurements specifies the reproducibility of the measurements under similar conditions and can be estimated in repeated measurements. High precision is associated with a small standard deviation of the distribution of the measurement results.

The accuracy of dosimetry measurements is the proximity of their expectation value to the "true" value of the measured

quantity. The inaccuracy of a measurement result is thus characterized by its uncertainty.

The uncertainty is a parameter that describes the dispersion of the measured values of a quantity; it is evaluated by statistical methods (type A) or by other methods (type B), has no known sign and is usually assumed to be symmetrical.

The standard uncertainty of type A, denoted u_A, is defined as the standard deviation of the mean value. It is obtained by a statistical analysis of repeated measurements and, in principle, can be reduced by increasing the number of measurements.

Type B standard uncertainties u_B are intelligent guesses or scientific judgments of nonstatistical uncertainties associated with the measurement (e.g., cannot be estimated by repeated measurements). These include calibration, influences on the measuring process (by temperature, humidity, etc.), application of correction factors or physical data taken from the literature.

The combined standard uncertainty u_C, associated with the quantity measured by the dosimetry system is thus a quadratic summation of the two uncertainties described above

$$u_C = \sqrt{u_A^2 + u_B^2}. \tag{29}$$

2) Linearity: Ideally, the dosimeter reading should be linearly proportional to the dosimetric quantity. However, often, beyond a certain dose range a nonlinearity sets in. The linearity range and the nonlinearity behavior depend on the type of dosimeter and, in general, a nonlinear behavior should be corrected for.

3) Dose Rate Dependence: Integrating systems measure the integrated response of a dosimetry system. For these systems, the measured dosimetric quantity should be independent of the rate of that quantity. Ideally, the response of a dosimetry system at two different dose rates should remain constant. In reality, the dose rate may influence the dosimeter readings and appropriate corrections would be necessary.

4) Energy Dependence: The response of a dosimetry system is generally a function of the radiation beam energy. Since dosimetry systems are usually calibrated at a specified radiation energy (and type) and usually used over a much wider energy range, the energy dependence of their response requires correction.

5) Directional Dependence: The variation in response of a dosimeter with the angle of incidence of radiation is known as the directional (or angular) dependence. Dosimeters usually exhibit directional dependence due to their construction, physical size, and the energy of the incident radiation. Dosimeters should then be used in the same geometry as that in which they are calibrated.

6) Spatial Resolution and Physical Size: Since the dose is a point quantity, the dosimeter should allow the determination of the dose from a very small volume. The position of the point where the dose is determined (i.e., its spatial location) should be well defined in a reference coordinate system. Certain dosimeters (such as the TLDs described later in Section III-D1) have very small dimensions and their use approximates a point measurement. Film dosimeters (Section III-C) have excellent 2-D resolution, while the point measurement is limited by the resolution of the readout system.

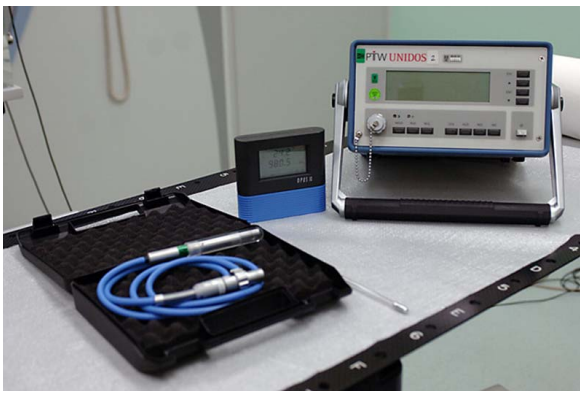

Fig. 9. Cylindrical (thimble type) ionization chamber and electrometers [13].

7) Readout Convenience: Direct reading or active dosimeters (e.g., ionization chambers or semiconductor dosimeters, described in Sections III-B and III-E, respectively) are generally more convenient than passive dosimeters (i.e., those that are read after processing following the exposure, as TLDs and films). Some other dosimeters are of the integrating type [e.g., TLDs and metal–oxide–semiconductor field-effect transistors (MOSFETs)]; others can measure in both integral and differential modes (ionization chambers).

8) Convenience of Use: Ionization chambers are reusable, with no or little change in sensitivity within their lifespan. Semiconductor dosimeters are reusable, but with a gradual loss of sensitivity within their lifespan. Some dosimeters are instead not reusable (e.g., Alanine in Section III-F1). Some dosimeters measure dose distribution in a single exposure (e.g., films in Section III-C), some others are quite robust (i.e., handling will not influence their sensitivity), while others are sensitive to handling (e.g., films).

B. Ionization Chamber Dosimetry

Ionization chambers are used for dose determination often in reference conditions (beam calibration). Air Kerma can be measured directly with an air-walled ionization chamber. At ^{60}Co energy, graphite cavity ionization chambers with an accurately known chamber volume are typically used as the primary standard (Section IV-A1).

Ionization chambers have a dynamic range from 10^4 to $\sim$1 Gy/s and come in various shapes and sizes, depending upon the specific requirements, but generally they are all basically a gas filled cavity surrounded by a conductive outer wall and having a central collecting electrode. The wall and the collecting electrode are separated with an insulator to reduce the leakage current when a biasing voltage is applied. The most popular design is the cylindrical type as shown in Fig. 9.

Measurements with air ionization chambers require temperature and pressure correction to account for the change in the mass of air in the chamber volume. An electrometer (device for measuring currents, shown in Fig. 9) is used in conjunction with the ionization chamber to measure the chamber current or charge collected over a fixed time interval.

For TID testing of electronics components, the parallel-plate ionization chamber design is of particular interest. It consists

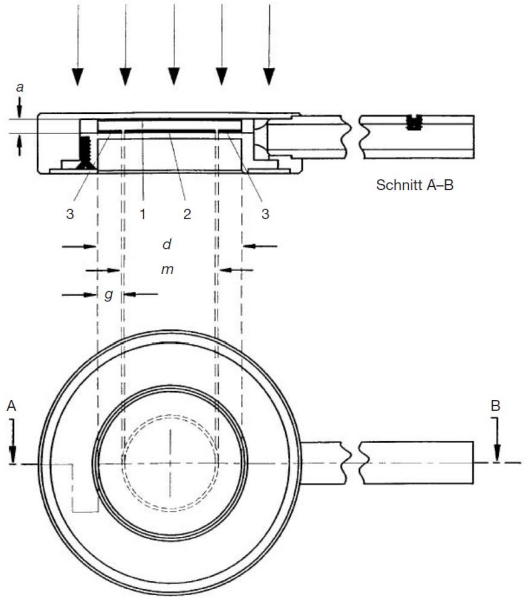

Fig. 10. Parallel-plate ionization chamber. 1: polarizing electrode, 2: measuring electrode, 3: guard ring, a: height (electrode separation) of the air cavity, d: diameter of the polarizing electrode, m: diameter of the collecting electrode, and g: width of the guard ring.

of two plane walls, one serving as an entry window and polarizing electrode and the other as the back wall and collecting electrode, as well as a guard ring system. The back wall is usually a nonconducting material [usually Polymethyl methacrylate (PMMA)] with a thin conducting layer of graphite forming the collecting electrode and the guard ring system on the top of it. A schematic of a parallel-plate ionization chamber is shown in Fig. 10.

The parallel-plate chamber is recommended for dosimetry of electron beams with energies below 10 MeV. Moreover, for TID tests on electronics performed in ^{60}Co sources (Section V-A), the low-energy photon component of the gamma spectrum can introduce significant dosimetry errors since the equilibrium dose, as measured by a dosimeter, can be quite different from the absorbed dose deposited in the DUT (dose enhancement effects described in Section IV-A2). The technique based on a specially fabricated parallel-plate chamber described in the test methods American Society for Testing and Materials (ASTM) E1250-10 [31] provides an easy means for estimating the importance of the low-energy photon component during a radiation test.

C. Film Dosimetry

PMMA (Perspex) dosimeter materials provide a means of directly estimating absorbed doses in near water equivalent substances, such as plastics, etc. Under the influence of ionizing radiation, chemical reactions within the material, creates or enhance absorption bands in the visible and/or ultraviolet regions of the spectrum. The optical absorbance determined at selected wavelengths, within the radiation-induced absorption bands, is quantitatively related to the corresponding absorbed dose. This technique, described in detail in [32], finds application in routine dosimetry mainly for radiation processing of

Fig. 11. Dual-wavelength photometer for readout of the FWT radiochromic dosimeters. The LED digital display reads directly in OD. The two wavelengths are 510 and 600 nm and are used to cover the range of the radiochromic dosimeters.

Fig. 12. GaF films radiotherapy type.

product and can still be a valid option for measuring relatively high doses in the TID range from 10^2 to $<10^5$ Gy. However, for TID testing of electronics components, this technique is superseded by the film dosimetry described in the following.

Radiochromic films contain a special dye that is polymerized upon exposure to radiation. The polymer absorbs light and the transmission of light through the film can be measured with a suitable densitometer, film (or flatbed) scanners, or a spectrophotometer [33] as the one shown in Fig. 11. A radiochromic film is self-developing and it requires neither developer nor fixer as does a radiographic film. Since it is grain less, it has a very high resolution and a reduced thickness; it can be conveniently used for dosimetry in high dose gradients.

The most commonly used films are the GafChromic (GaF) films. Several types of films, in which the sensitive medium is coated with different substrate layers of various materials and thicknesses, are available on the market [34]. An example of radiotherapy-type film [35] for the dosimetry of a particle beam is given in Fig. 12. The optical density (OD) of these films usually increases with time, reaching saturation less than 24 h after exposure [36].

Dosimetry with radiochromic films has a few advantages over old radiographic films, such as ease of use, elimination of the need for darkroom facilities, film cassettes or processing, dose rate independence, and better energy characteristics (except for low-energy X-rays below 25 kV), although they need to be protected from extreme environmental conditions (e.g., excessive humidity or high temperature). Radiochromic films are useful at higher doses, from the Gy up to several hundreds of kilogray, as the type FWT-60 from Far West Technology Inc., Goleta, CA, USA [37], although nonlinearity

TABLE I
CHARACTERISTICS OF THE RADIOCHROMIC FILMS

Type	Configuration	Substrate	Active Layer	Dynamic Range
GaF XR-RV3	4-layer (231μm)	Polyester	17μm	0.1-500cGy
GaF HD-V22	2-layer (109μm)	Polyester	12μm	10-1000Gy
GaF MD-V3		Polyester		1-100Gy
FWT-60	1-layer	Nylon	~40μm	0.5-200kGy

of the dose response should be corrected for in the upper dose region.

A radiochromic film is a relative dosimeter. If proper care is taken with the calibration and the environmental conditions, a precision better than 3% is achievable [38]. Data on the various characteristics of radiochromic films (e.g., sensitivity, linearity, uniformity, reproducibility, and post-irradiation stability) are available online [39]. The most commonly used film types for TID measurements are summarized in Table I.

Such thin films can be conveniently used in the determination of the dose released by, weekly penetrating, low-energy X-rays. However, in all practical cases for electronic components, this dose measured with films need to be converted into the one delivered by the broad X-ray photon energy spectrum (as the one shown in Fig. 1) in an equivalent thickness of Si or SiO_2 placed at the same location of the film dosimeter. An example of this type of calculation is detailed step-by-step in [40].

D. Luminescence Dosimetry

Some materials, upon absorption of radiation, retain part of the absorbed energy in metastable states. When this energy is subsequently released in form of UV, visible or IR light, the phenomenon is called luminescence. Two types of luminescence, fluorescence and phosphorescence, are known which depend on the time delay between stimulation and the emission of light. Phosphorescence occurs with a time delay exceeding 10^{-8} s. The process of phosphorescence can be accelerated with a suitable excitation.

1) In the form of heat, the phenomenon is known as thermoluminescence (TL) and the material is called a TLD when used for dosimetry.
2) In the form of light, the phenomenon is referred to as optically stimulated luminescence (OSL).

In a crystalline solid, the electrons produced in the primary interactions of photons or charged particles release numerous low-energy-free electrons and holes through ionization. These free carriers will thus either recombine or become trapped in an electron or hole trap, respectively, somewhere in the crystal. The traps can be intrinsic or introduced in the crystal in the form of lattice imperfections consisting of vacancies or impurities. Two types of traps are known in general: storage traps and recombination centers.

A storage trap localizes free charge carriers and releases them during the subsequent heating, resulting in the TL process, or irradiation with light, resulting in the OSL process.

Fig. 13. TLD chips (bottom); the standard holder hosting the TLD chips during their readout.

A charge carrier released from a storage trap may recombine with a trapped charge carrier of opposite sign in a recombination (luminescence) center. The recombination energy is always partially emitted in the form of light that can be measured with photodiodes or photomultiplier tubes (PMTs).

1) Thermoluminescent Dosimeter Systems: The most commonly TLDs used in dosimetry are sintered LiF:Mg,Ti (MTS-7) and LiF:Mg,Cu,P (MCP-7). Both are based on lithium fluoride with ^{7}Li, hence the nomenclature MCP-7 and MTS-7 given above. However, because of their different dopant compositions, they have different dosimetric properties, like sensitivity, nonlinearity of dose response and efficiency when measuring dose delivered by hadrons [41].

Two types of TLDs, named MCP-N and MTS-N also exist. They feature an enriched component of ^{6}Li, which makes this material more sensitive to thermal neutron radiation. Other TLDs, used because of their high sensitivity, are $CaSO_4$:Dy, Al_2O_3:C, or CaF_2:Mn.

TLDs are available in various forms (e.g., chips, as shown in Fig. 13) and before use they need to be annealed to erase the residual signal. The TL intensity emission is a function of the TLD temperature T: keeping the heating rate constant makes the temperature T proportionally increasing with time and so the TL intensity can be plotted as a function of time. The resulting curve is called the TLD glow curve [42]. The peaks in the glow curve may be correlated with trap depths responsible for TL emission. For instance, in dosimetry the main dosimetric peak of the MTS glow curve between 180 °C and 260 °C is used (see Fig. 14). This peak temperature is high enough so as not to be affected by room temperature (RT). The total TL signal emitted (e.g., the area under the glow curve) can be correlated with dose through proper calibration. Therefore, a good reproducibility of heating cycles during the readout is important for accurate TLD dosimetry.

MTS crystals have been used for standard dosimetry for many decades. For dose levels >1 Gy, their radiation response becomes supralinear and has to be corrected accordingly. MCP dosimeters were developed later and they exhibit higher sensitivity to radiation by a few orders of magnitude, with the drawback of having lower sensitivity for heavy charged particles. Opposite to MTS, the MCP response becomes sublinear

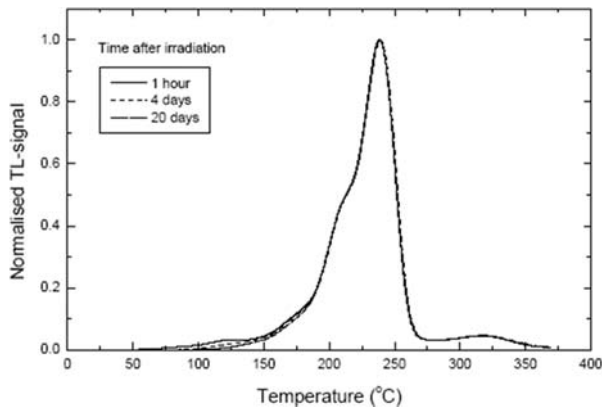

Fig. 14. MTS-7 glow curve with main peak between 180 °C and 260 °C [13].

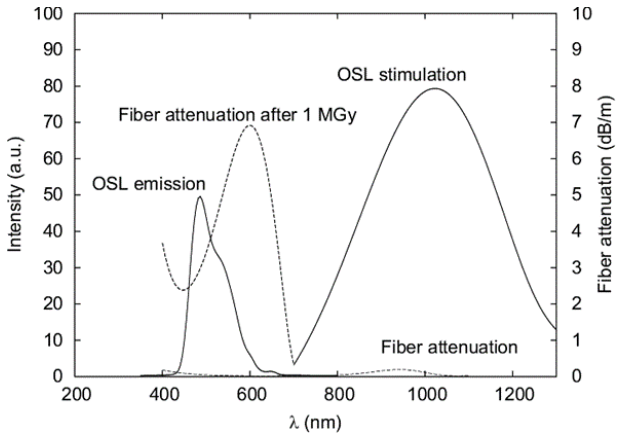

Fig. 15. SrS:Ce,Sm emission and stimulation spectra for an OSL material embedded in an optical-fiber system (left-hand axis, continuous lines) [43]. Attenuation in the optical fiber (dB/m) due to radiation damage (right-hand axis, dashed lines).

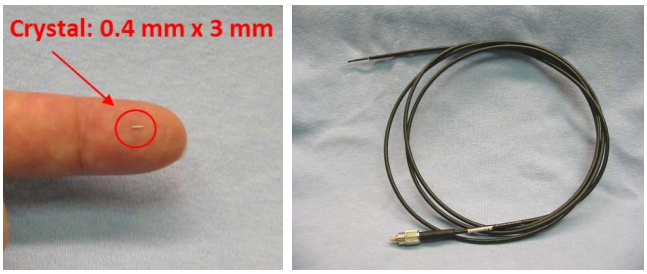

Fig. 16. Example of a dosimetric probe based on an OSL crystal (left) coupled with an optical fiber (right) [13].

above 1 Gy, which similarly calls for a correction factor when converting signal to dose [41].

The TL signal decreases in time after the irradiation due to spontaneous emission of light at RT. This process is called fading. Typically, for MTS-7, the fading of the dosimetric peak does not exceed a few percentages over several months at RT. This almost negligible fading makes TLD dosimetry very accurate in the range of 10^{-5}–10 Gy within an error of 5% [43].

In these recent years, efforts have been made by scientists at the Henryk Niewodniczański Institute of Nuclear Physics (IFJ PAN), Krakow, Poland, to extend the measuring range of the TL dosimeters to a few orders of magnitude above their traditional maximum limit. They demonstrated that, with appropriate corrections, the main luminosity peaks of the readout of MTS detectors can be used to measure dose up to a maximum of about 1 kGy. MTS sensors that are exposed to a dose of more than 1-kGy saturate and are considered to be outside of their sensitive range. Moreover, it has been demonstrated that a single MCP detector can be used to measure TID up to 1 MGy, by introducing a parameter called the ultrahigh temperature ratio [44].

2) Optically Stimulated Luminescence Systems: OSL is based on a principle similar to that of TL dosimetry. Instead of heat, light (often from a laser) is used to release the trapped energy in the form of luminescence. The integrated dose measured during irradiation can be evaluated using OSL directly afterward.

Although the carbon-doped aluminum oxide (Al_2O_3:C) is now the standard material in a wide range of OSL applications, other materials exist. For TID testing and space dosimetry the SrS:Ce,Sm has been extensively used [45], [46]. The optimum stimulation wavelength for this material lies around 1 μm. The advantage of this material compared to aluminum oxide is that the optical stimulation results completely independent and easy to discriminate from the emission spectrum that instead ranges from 450 to 650 nm [47], as shown in Fig. 15.

An optical fiber OSL dosimetry system consists typically of a small ($\sim$1 mm^3) chip of Al_2O_3:C coupled with a long optical fiber (see Fig. 16), a laser, a beam splitter, a collimator, a PMT, electronics, and software. To produce OSL, the chip is excited with laser light through the optical fiber and the resulting luminescence (blue light) is carried back in the same fiber, reflected of 90° by the beam splitter and measured in a PMT.

The optical fiber dosimeter exhibits high sensitivity in the range of 10^{-5}–10^2 Gy over a wide range of dose rates. The OSL response is generally linear and energy independent as well as the dose rate, although the angular response requires correction.

Sometimes, in practical dosimetry systems, OSL is used in conjunction with radioluminescence which is emitted promptly and provides information on the dose rate during irradiation, while OSL provides the integrated dose thereafter [48].

E. Semiconductor Dosimetry

1) Silicon Diode Dosimetry Systems: A silicon diode dosimeter (see Fig. 17) is a p-n-junction diode. The diodes are produced by taking n-type or p-type silicon and counter doping the surface to produce the opposite type material. These diodes are referred to as n–Si or p–Si dosimeters, depending upon the base material. Both types of diode are commercially available, but the p–Si type is more suitable for dosimetry, since it is less affected by radiation damage and has a much smaller dark current.

Radiation produces e–h pairs in the body of the dosimeter, including the depletion layer. The charges (minority carriers) produced within the diffusion length diffuse into the depleted region and are swept across it under the action of the electric

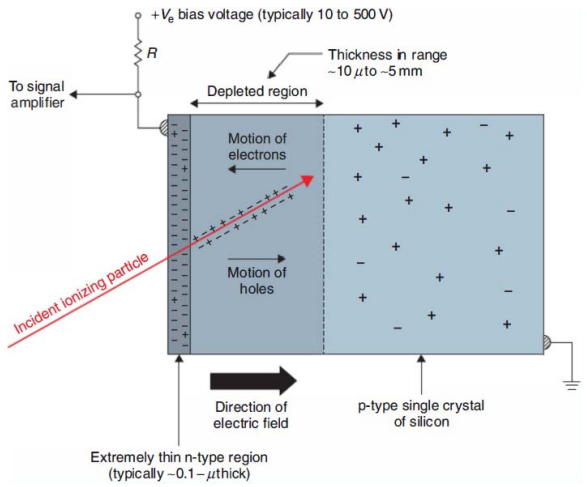

Fig. 17. Cross section of a silicon diode dosimeter [13].

field, due to the intrinsic potential. In this way, a current is generated in the reverse direction in the diode.

Diodes are used in the short circuit mode, because this exhibits a linear relation between the measured charge and the dose. The size of the intrinsic region in the diode depends more on the diode construction than on the reverse bias. Thus, the sensitive volume is only a weak function of the applied voltage, making the diode relatively insensitive to voltage variations. Often, they are even operated without an external bias to reduce leakage current [49].

Diodes are more sensitive and smaller than typical ionization chambers and can cope with very high dose rates up to 10^8 Gy/s. They are relative dosimeters and should not be used for beam calibration, since their sensitivity changes with repeated use due to radiation damage. Moreover, diodes can be constructed with a variety of semiconductor materials (Si, GaAs, etc.) matching the material of interest for electronics components testing. They show variations in their response with temperature, dose rate, as well as angular and energy dependence.

Because of their fast time response (ns time scale), silicon diodes are suitable for dosimetry measurements in pulsed radiation fields, e.g., for flash X-rays or electron LINACs.

2) MOSFET (RadFET) Dosimetry Systems: A MOSFET, a miniature silicon transistor, possesses excellent spatial resolution and offers very little attenuation of the beam due to its small size. MOSFET dosimeters (also called RadFETs) are based on the measurement of the transistor threshold voltage, which is a function of the TID [50], [51].

Ionizing radiation penetrating the gate oxide generates charge that is permanently trapped, thus causing a change in the transistor threshold voltage [52], as shown in the MOS cross section in Fig. 18. The integrated dose can be measured by forcing a dc current into the device and measuring the dc voltage, during or after irradiation, with a properly designed electronic circuit [53], [54].

MOSFETs can be exposed with the gate unbiased for the measurement of high TID levels (up to 100 kGy as shown in Fig. 19) or may require a connection to a bias voltage during irradiation to reach sensitivities in the mGy range. These

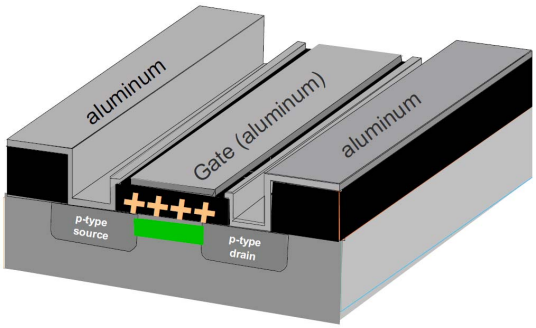

Fig. 18. RadFET cross section and location of the trapped charge [52].

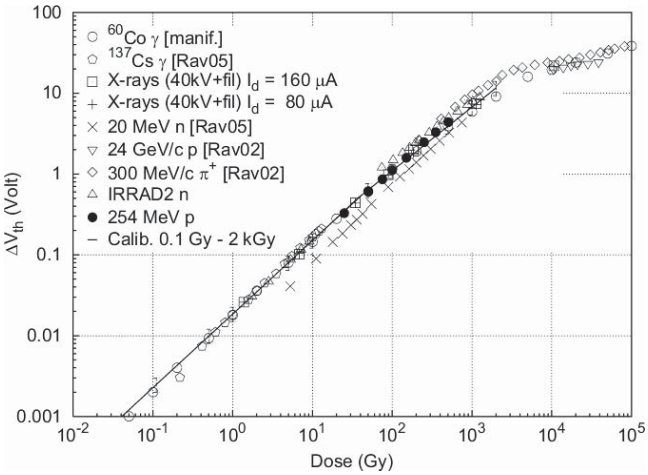

Fig. 19. Typical radiation response of REM RadFET TOT-501C Type K with $t_{ox} = 0.25$ μ m. The RadFET threshold voltage shift in volts, recorded unbiased, is plotted versus the TID expressed in Gy [43].

transistors can be embedded in different packaging solutions depending on the measurement application [55], [56].

A single MOSFET dosimeter can cover the full energy range of photons and electrons, although the energy response should be examined, since it varies with radiation quality. For megavoltage photon beams, however, MOSFETs do not require energy correction and a single calibration factor can be used [57]. MOSFETs exhibit small axial anisotropy (±2% for 360°) and do not require dose-rate corrections. Similar to diodes, a single MOSFET exhibits a temperature dependence, but this effect can be limited (corrected for) of overcome by specially designed double detector MOSFET systems [58].

In general, MOSFET dosimeters show nonlinearity of response with the total absorbed dose as shown in Fig. 19; however, over a specified dose range, they retain adequate linearity. MOSFETs are also sensitive to changes in the gate bias voltage during irradiation (it must be stable) and their response drifts slightly after the irradiation (readings must be taken at a specified time after applying the dc current) [43].

F. Other Active and Passive Dosimetry Systems

1) Polymer Alanine Dosimeter (PAD): Alanine is an aminoacid showing chemical composition $CH_3 \cdot CH(NH_2) \cdot COOH$. PADs are typically used for high-dose dosimetry in

Fig. 20. Alanine dosimeter samples shaped in form of pellets [13].

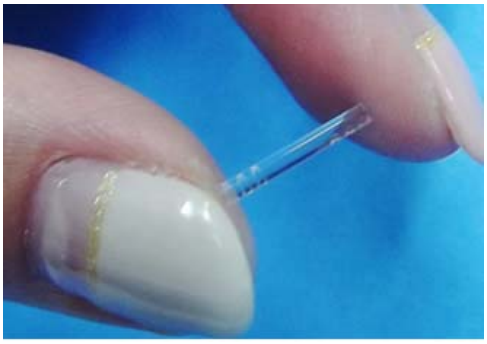

Fig. 21. RPL dosimeter sample [13].

Fig. 22. Comparison of the top surface of a damaged crystal (left) versus an intact crystal with a smooth surface (right) [64].

the TID range from 10 to 10^5 Gy. However, it has been demonstrated that an accuracy down to 10^{-2} Gy can be achieved with PADs using a particular readout technique [59]. PADs can be shaped in the form of rods or pellets (see Fig. 20) with an inert binding material. At CERN, for instance, they are manufactured in form of small cables where the alanine powder (67%) is mixed to a polymer (33%) that act as binder to give them a compact cylindrical form of about 20 mm in length and 4 mm in diameter. This characteristic makes the alanine easy to be inserted in places difficult to access.

When Alanine is exposed to ionizing radiation, radicals are generated which can be measured using an electron spin resonant (ESR) spectrometer. The concentration of the stable radical CH_3-$C^{\cdot}$H-COOH, which is predominant at RT, gives a prominent pattern that grows linearly with the dose absorbed by the dosimeter [60]. The intensity is measured as the peak-to-peak height of the central line in the ESR spectrum. The readout is nondestructive making these dosimeters not reusable.

Alanine is tissue equivalent and requires no energy correction for γ-rays of energies >120 keV [43]. It exhibits very little fading for many months after irradiation. The response depends on environmental conditions during irradiation (temperature) and storage (humidity). Although alanine can also be used as a reference standard (Section IV-A1) [61], the typical precision achievable measuring the TID for electronic testing is on the order of 10%.

2) Radio-Photoluminescence (RPL) Dosimeters: Ionizing radiation induces stable RPL centers in silver-activated aluminophosphate glass, which emit phosphorescence when exposed to UV light (∼365 nm). The amount of the phosphorescence is related to the amount of radiation absorbed in the glass [62]. The light output increases linearly with the dose up to about 100 Gy, then the calibration curve reverses at about 1 kGy due to the increase of the coloration and the corresponding self-absorption of the glass. These dosimeters are typically used in form of small transparent cylinders of 6-mm length and ∼1-mm diameter as shown in Fig. 21. RPLs allow measurements in a broad dose range from 0.1 Gy to 1 MGy; however, they present a large overestimation in the measured dose for low-energy photons ($E < 500$ keV). Small fading, on the order of a few percentages over three months, has been measured for RPL at RT [63].

The precision achievable in measuring the ionizing dose with RPLs is on the order of 20% for doses up to some hundreds of gray. At higher doses (kGy range), the reversed behavior of the calibration curve makes the measurement uncertainties bigger.

High-temperature annealing of RPL can erase the dosimetric information allowing their reutilization. However, this has been recently found at CERN to be a potential problem for long-term usage [64]. A wide variety of damages (cracked and splintered surfaces) has been found on RPL samples reused many times over the years. An example is shown in Fig. 22. This kind of damage is influencing the readout process. During the readout, the crystals are illuminated with UV light in order to stimulate the light emission. Due to the geometry of the measurement setup, cracked or bent surfaces can influence the amount of light that reaches the photo sensor (usually a PMT) by reflection.

3) Plastic Scintillator Dosimetry System: Plastic scintillators are a relatively new development in dosimetry. The light generated in the scintillator during its irradiation is carried away by an optical fiber to a PMT, located outside the irradiation room.

Plastic scintillators are characterized by dose linearity, good reproducibility and long-term stability. Scintillators suffer no significant radiation damage (up to about some tens of kilogray), although the light yield should be monitored when used. They are also dose rate, direction, and nearly energy independent and can thus be used directly for relative dose measurements. The useful dose-rate range is 10^4–10^9 Gy/s. Plastic scintillators can be made very small (about 1 mm^3 or less) and yet give adequate sensitivity for dosimetry [65]. They can be conveniently used as dose-rate detectors for high-energy flash X-ray sources ($E > 300$ keV) and should be

considered whenever the required sensitivity compares with the one offered by silicon diodes (Section III-E1). Because these detectors produce an output signal of several hundreds of volts, they are quite immune to electromagnetic noise which is a common problem at flash X-ray facilities [49].

4) Diamond Dosimeters: Diamonds change their resistance upon radiation exposure. When applying a bias voltage, the resulting current is proportional to the dose rate of radiation. Commercially available diamond dosimeters are designed to measure relative dose distributions in high-energy photon and electron beams and have a typical response of few nC/Gy [66].

Diamonds have a small sensitive volume (a few mm^3) which allows the measurement of dose distributions with an excellent spatial resolution. Moreover, they feature a flat energy response and negligible directional dependence, which makes them well suited for use in high dose gradient regions. In order to stabilize their dose response, they should be irradiated (with a few Gy) prior to each use to reduce the polarization effect. In addition, they have a negligible temperature dependence, high sensitivity, and resistance to radiation damage.

G. Particle Beam Monitoring Devices

Radiation testing of electronics using proton energies ranging from 10 MeV to several GeV can be done in air. Proton testing at energies below 10 MeV must be carried out in vacuum adding complications that will not be addressed in this paper.

Beam facilities, as the one used for proton irradiation, rely on three primary dosimetry systems to determine the flux and uniformity of the beam.

1) scintillators (usually plastic/organic);
2) secondary electron monitors;
3) Faraday cups.

These systems can be calibrated in absolute terms, for instance, by means of the activation foils technique (discussed later in Section III-G4). In addition, radiochromic films (Section III-C) may also be used to determine qualitatively the uniformity of a particle beam.

The beam intensities for simulating space, terrestrial and HEP radiation effects range from approximately 10^2–10^{11} p/cm^2/s. This large range is due to the very diverse needs of the community: from low-dose SEE studies to TID measurements in optical components.

The dosimetry at most proton accelerators is reasonably accurate, at least within 10% [5], although for electronics testing the proton fluence should be determined, ideally, to better than 5% (Section IV-D). A proton beam should also be nearly monoenergetic ($\Delta E/E < 5\%$) and its energy should be known to better than 2%–5%, depending on the application [67].

It should also be mentioned that, for low-energy proton beams, if a degrader is positioned in front of the DUT, the dosimetry is altered. The user must make the necessary corrections to allow for the broadening and shifting of the peak in the energy spectrum as a result of energy loss that depends on the type of material used in the degrader, as well as its thickness (Section IV-A3).

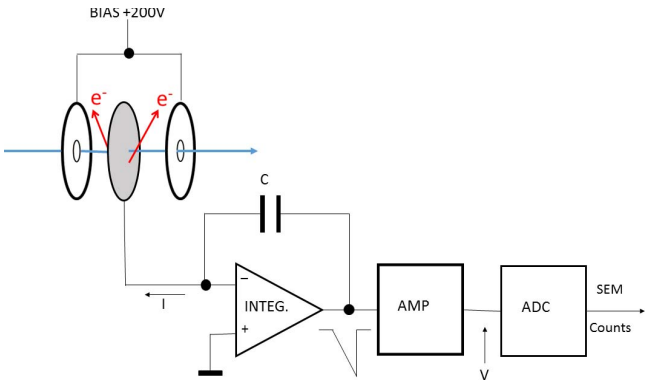

Fig. 23. Secondary emission monitor principle and readout electronics.

1) Scintillators: A scintillator detector converts a portion of the incident particle energy into light (as described previously in Section III-F3). The scintillator response is directly proportional to the energy lost by the incident particle. A typical plastic scintillator consists of a solid transparent solvent (polyvinyl toluene) containing a scintillator (p-terphenyl which emits light at 340 nm) plus a wavelength shifter (p, p'-diphenyl stilbene) which absorbs the light from the scintillator and reemits it at a wavelength of 408 nm which is better matched to the photodetector response [14].

Photons produced in the interaction are detected typically by a PMT, which produces a current proportional to the light intensity. The final result is a detectable electrical signal from even a single photon [68]. These types of scintillators are often custom-made directly by the proton irradiation facility.

2) Secondary Electron (Emission) Monitors: These detectors function by passing the beam through a series of thin metal films (e.g., aluminized Mylar). Interaction with the beam knocks secondary electrons free in the aluminum foils, which are tied to a charge-integrating circuit as shown in Fig. 23. The current is proportional to the number of particles passing through the foils and often converted into counts. For this reason, these devices are also commonly refereed as secondary emission counters [69].

An alternate setup that allows for the determination of the profile of the beam is possible as well. The foils are arranged such that alternating foils are positively biased and the foils for detection are sandwiched in between these foils. These latter are only aluminized on the top, bottom, left, or right half. The display of the readings of each foil allows the operator to determine the beam uniformity and focus [70]. When the energy and the intensity of the beam are high enough, the foils can be arranged with a pixelated layout and measurable currents can be obtained, even without applying a bias. This makes a simple and cost-effective monitor, which can be used for beam profile (or position) measurements in HEP facilities, as it is implemented at the CERN IRRAD proton facility [71], [72].

3) Faraday Cup: The Faraday cup is essentially a well surrounded by a magnetic field designed to capture the entire beam. In the case of protons, for each ion entering the cup, an electron is pulled from ground through a current meter.

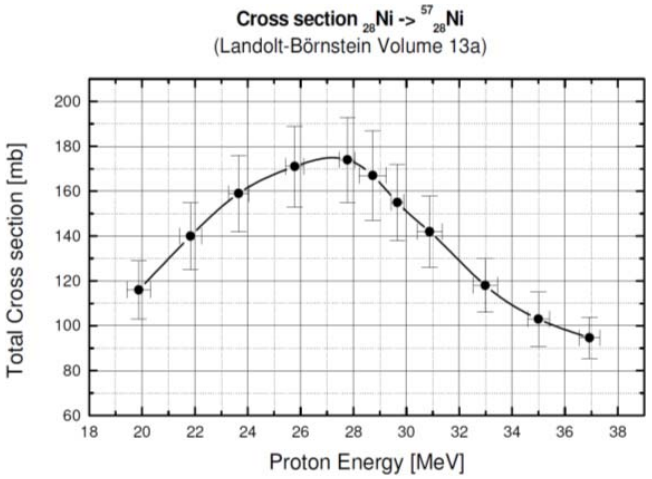

Fig. 24. Cross section of ^{58}Ni $\rightarrow$ ^{57}Ni used to determine the fluence of 10-MeV protons. The dominating γ-line at 1377.6 keV is used to determine the activity of ^{57}Ni [74].

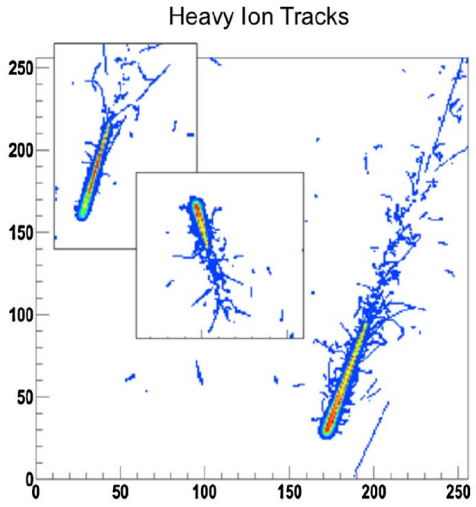

Fig. 25. Series of galactic cosmic rays ion tracks from ISS as measured by the Timepix radiation monitor [79].

The magnetic field around the cup prevents secondary electrons inside the cup from escaping, as well as prevents anyone produced externally from entering. Since this measurement is destructive, Faraday cups are designed to be moved in and out of the beam or are placed in a separate area to provide measurements only when needed, and can be used for electron beam with energies up to some hundreds of megaelectronvolt [73].

4) Activation Foils: This method for absolute particle fluence measurements is based on nuclear reactions that lead to the formation of radionuclides in thin foils of various high-purity materials (Al, Au, Co, In, Ni, etc.). After the foil is exposed to the particles, the amounts of generated radionuclides (their activity) can be determined by means of gamma spectroscopy analysis with opportune corrections to take into account the radionuclide decay constant (Section II-A) and the thickness of the material foil. The foil weight and shape is selected according to the particle flux intensity and irradiation time. The calculation of the specific activities induced in the materials provides information about the particle flux in different energy ranges by using specific cross sections as shown in Fig. 24 [62], [74]. In this calculation, the irradiation time and the half-lives of different isotopes must be taken into account to evaluate the specific activity at saturation.

With this method, particle fluence can be determined with an accuracy of a few percentages [75]. For charged particle fluence measurements, some cross sections of interest for protons are given in [76] and [77].

H. Other Devices

In this section, some other technologies of dosimeters, which may be useful mostly for radiation field or particle beam characterization, are briefly discussed.

1) CERN Medipix and Timepix: Medipix is a family of readout chips for particle imaging and detection, developed at CERN by the Medipix Collaborations [78]. These chips, used as a part of pixelated hybrid detectors, work like a camera, detecting and counting each individual particle hitting the pixels when its electronic shutter is open.

In particular, the Timepix devices with a 256×256 pixel matrix have been designed for recording radiation quanta in a variety of semiconductor sensor materials (Si, diamond, GaAs, etc.) or also in a gas volume. During a programmable exposure time (from μs to hours) each pixel can measure the amount of energy deposited in its volume or attribute a time stamp to the first hit, also down to ns scale, with respect to the end of the exposure. The pixels are 55 μm^2 and the charge carriers generated in the sensor spread over a number of adjacent pixels. This geometric spreading of these charge carriers results in a cluster of hit pixels with a shape that is typical for the type of incident radiation [79]. As long as the clusters can be separated and identified, either visually or by pattern recognition algorithms, the Timepix device allows thus to resolve the quanta that constitute the mixture of incident ionizing radiation (method also referred as "quantum dosimetry") [80]. An example of heavy ion tracks measured by the Timepix device in space is shown in Fig. 25.

One of the advantages of the Timepix device is its sensitivity to incident alpha particles, while at the same time electrons and low-energy X-rays are detected with good efficiency. For high-energy X-ray or γ-ray, the efficiency is relatively lower, so that larger areas, converters, or longer exposure times are needed, depending on the required precision in dosimetry applications.

Radiation monitors based on Timepix have been tested successfully for monitoring the radiation environment aboard the International Space Station (ISS) [81]. The research and development on these sensors continue in order to be able to supply a direct translation of this detailed "quantum" information into a traditional value for the corresponding dose, as it would be determined using the classical dosimetric techniques described in Section III [82].

2) Floating-Gate Dosimeters: Floating-gate MOSFETs (FG MOSFETs) [83] were initially conceived for the implementation of cells in nonvolatile memories. Afterward, due to

their sensitivity to radiation, both nonvolatile memories and standalone FG MOSFETs were proposed as dosimeters.

FG MOSFETs can be manufactured in any conventional complementary metal–oxide–semiconductor process and provide good sensitivity for zero bias operation. Charges can be placed on the floating capacitor, prior to the irradiation, through an injector. Then, radiation reduces the charge in the FG by means of two effects: first, the injection in the floating gate of the charge generated in the surrounding oxides and second, the photoemission of carriers (which get enough energy to overcome the potential barrier) from the FG. The capacitor can be charged back to the initial value, giving the possibility to reuse it several times [84].

FG MOSFETs dosimeters are suitable for space applications [for TID up to tens of krad(Si)] and popular thanks to their consolidated manufacturing process, their reduced size, the possibility of integrating the readout electronics, and their low-voltage supply requirements.

IV. Issues in TID Measurements

A. Factors Affecting the Dose Measurements

1) Dosimeters Calibration: Calibration of a routine dosimetry system can be carried out directly in a national or accredited standards laboratory. Alternatively, as it happens often in dosimetry for TID testing, it may be carried out through the use of a local (in-house) calibration facility or in a production irradiator. All possible factors that may affect the response of dosimeters, including environmental conditions, should be known and taken into account. The associated instrumentation to the dosimetry system (e.g., as the densitometer for the readout of radiochromic films described in Section III-C) must also be calibrated.

Dosimeters may be divided into three basic classes in accordance with their relative quality and areas of applications.

1) Primary–Standard Dosimeters are established and maintained by national standards laboratories for calibration of radiation fields. Primary–standard dosimeters are typically used to calibrate or intercompare radiation environments in dosimetry calibration laboratories, and are not normally used as routine dosimeters. The two most commonly used primary–standard dosimeters are ionization chambers and calorimeters (not covered in this paper).
2) Reference–Standard Dosimeters are used to calibrate radiation environments and to calibrate routine dosimeters. Reference–standard dosimeters may also be used in routine dosimetry applications for radiation processing [61]. Widely used reference dosimeters include the alanine dosimetry (see ISO/ASTM Practice 51607 [85] and Section III-F1).
3) Routine Dosimeters are used in radiation processing facilities for absorbed-dose mapping and process monitoring. The majority of the techniques listed in Section III belong to this class.

More information on the selection and calibration of the dosimeter classes listed above can be found in the ISO/ASTM Practice 51261 [86].

2) Absorbed-Dose Enhancement Near Material Interfaces: Most semiconductor devices can be represented as a 1-D planar layer of active and structural materials. One phenomenon, which is of crucial importance to the process of deducing the absorbed dose in a region of interest in a device from an equilibrium dose measurement made by a dosimeter, is the interface absorbed-dose enhancement [87]. Strong dose enhancement effects occur in semiconductor devices when there are high-Z materials in the device structure. In semiconductor parts, high-Z materials can occur in the chip metallization or in the device package [88]. A common example would be a device with a gold layer packaged on the inside of a Kovar lid. New generation of packages for microelectromechanical system devices (flip chip, ball grid array, etc.) can be sensitive to the same effect, therefore, the same precautions applies in TID testing as indicated in the standard test procedures [8], [89]. The energy deposition by secondary electrons produced by photons near the interface between layers depends, in a complex way, on the following:

1) effective atomic number of the layers;
2) photon energy/direction;
3) layer thickness.

and may require to be studied with dedicated simulation tools (Section II-F4) [90].

The dose enhancement effect at the interface at low-photon energies (about 10–200 keV, typical of X-ray facilities) is strongly dependent on the energy and the material Z, and is not very dependent on the direction of incident photons. This effect can extend over a region of the order of hundreds of nanometer from the interface [91], [92].

The dose enhancement effect at high-photon energies ($\geq$1 MeV) is not strongly dependent on photon energy or the materials Z; however, it is strongly dependent on the direction of the incident photons. At such energies, the effect extends over a region of hundreds of micrometer from the interface [30], [93].

3) Energy Spectrum Hardening and Softening: Photons can be scattered from other materials on their path from the source location to the region of interest within the DUT. Such intervening materials will add low-energy photons to the overall spectrum through Compton scattering and will remove low-energy photons from the spectrum through photoelectric absorption.

High-Z materials (such as lead) tend to harden the spectrum. Low-Z materials (such as Al or water) tend to soften the spectrum. A soft spectrum is typically caused by Compton scattering from low atomic number materials. It is particularly important in water well sources, if long water paths are used, and in room sources, if there is significant photon backscattering from walls and floors.

For TID testing with protons, if a degrader is positioned in front of the DUT, the dosimetry is altered. The user must make the necessary corrections to allow for the broadening and shifting of the peak in the energy spectrum as a result of energy loss that depends on the type of material used in the degrader as well as its thickness. More details on the use of degraders in proton beams are available in [5].

4) Conversion of Dosimeter Dose to Device Dose: This has to be performed using (23) and (24) given in Section II-F. The use of these equations (without a correction for absorbed dose enhancement effects) gives good accuracy when the volume of interest is sufficiently far from interfaces, or where interface regions form a negligible fraction of the volume of interest. The thickness of the region, where absorbed-dose enhancement effects are important, is dependent on the range of Compton electrons and photoelectrons produced in the energy deposition processes.

The thickness of the absorbed-dose enhancement region for a ^{60}Co irradiation is of the order of hundreds of micrometer. Therefore, for example, in MOS devices where the critical gate oxide is 10–200 nm thick, the volume of interest will generally lie within the enhancement region.

Since mass–energy absorption coefficients are a function of photon energy, the use of the previous equations requires knowledge of the incident photon spectrum. However, for photon energies >250 keV, ratios of mass–energy absorption coefficients are slowly varying functions of photon energy. Therefore, the errors introduced by this approximation are usually less than about 10% (Section II-F1). Another consideration in absorbed-dose conversion is that the photons will generally have passed through different layers of material in going from the source to the dosimeter compared to going from the source to the DUT. Therefore, the energy spectrum incident on the dosimeter will be different from that incident on the device. For ^{60}Co irradiations of electronic devices, these differences can be neglected if care is taken to make the irradiation geometry of the dosimeters and devices essentially the same. The resulting dosimetry errors are generally less than 10%.

By following published standard practices and the test standard (Section IV-D), it is possible to minimize these errors affecting the dosimetry measurements.

B. Factors Affecting the Dosimeter Response to Radiation

Several factors can contribute to the uncertainty in the measurement of absorbed dose for a specific dosimetry system. Because of the diverse types of dosimeters covered in this paper, the most important factors have been detailed in Section III for every described dosimeter. A useful summary of the most common factors is available in [86].

C. Errors and Uncertainty

The guide ISO/ASTM 51707:2005 [94] defines possible sources of uncertainty in dosimetry performed in γ-ray, X-ray, and electron irradiation facilities, and offers procedures for estimating the resulting uncertainties in the measurement of the dose using a given dosimetry system. A combined standard uncertainty $\leq 20\%$ is typically acceptable in TID measurements for electronics testing.

D. Dosimetry for TID in Radiation Standards and Guidelines

1) ESCC 22900: According to ESCC 22900 [7], the radiation field used for TID testing shall be a ^{60}Co source or an electron accelerator beam. Alternative sources that can be correlated with these sources may be used but, in the case of dispute, ^{60}Co or electron accelerator methods shall govern. The dose at the DUT shall be measured to a resolution of better than 10% and the nonuniformity of the radiation field in the test area shall be a maximum of 10%. The field uniformity shall be verified if the geometry of the test setup is changed. The dose rate of a ^{60}Co source shall be calibrated in accordance with the requirements of ESCC basic specification number 21500 to 5% or better [95].

Dosimetry shall be traceable to national standards. Corrections for source decay shall be made once per month. Test specimens shall be surrounded by an equilibrium material. This layer will minimize dose enhancement from low-energy scattered radiation by establishing CPE conditions. If it can be demonstrated that low-energy scattered radiation does not cause dosimetry errors due to dose enhancement, then the equilibrium material may be omitted. For equilibrium, the use of a container of at least 1.5-mm Pb with an inner lining of at least 0.7-mm Al is recommended.

The electron source used for the test shall be a steady-state type. The electron energy shall be sufficient to penetrate the package and shall be ≥ 1 MeV at the semiconductor die. The electron beam shall be monitored with a Faraday cup and a current integrator. Alternative monitoring methods may be used, but, in the case of dispute, the Faraday cup and current integrator method shall govern. In the case of ionization effects, the fluence for a given electron energy shall be accurately converted to Gy(Si) at chip level, taking into account potential dose enhancement effects due to the component's package, high-Z materials, etc. The dose profile of the beam shall be uniform within $\pm 10\%$ for a distance of at least 24 mm or 5 times the chip diagonal, whichever is the greater.

2) MIL-STD-883 Method 1019.9: This test procedure defines the requirements for testing packaged semiconductor ICs for TID effects from a ^{60}Co gamma ray source. In addition, this procedure provides an accelerated aging test for estimating low dose-rate ionizing radiation effects on devices. This aging test is important for low dose rate or certain other applications in which devices may exhibit significant time-dependent effects. This procedure addresses only steady-state irradiations and is not applicable to pulse type irradiations.

According to MIL-STD-883 [8], the radiation source used in the test shall be the uniform field of a ^{60}Co source. Uniformity of the radiation field in the volume where devices are irradiated shall be within $\pm 10\%$ as measured by the dosimetry system, unless specified otherwise. The intensity of the gamma ray field of the ^{60}Co source shall be known with an uncertainty below 5%. Field uniformity and intensity can be affected by changes in the location of the device with respect to the radiation source and the presence of radiation absorption and scattering materials.

An appropriate dosimetry system capable of carrying out the measurements specified in the standard shall be provided. The following ASTM standards or other appropriate standards shall be used.

1) *ASTM E666:* standard method for calculation of absorbed dose from gamma or X radiation [40].

2) *ASTM E668:* standard practice for the application of TLD systems for determining absorbed dose in radiation hardness testing of electronic devices [25].
3) *ASTM E1249:* minimizing dosimetry errors in radiation hardness testing of silicon electronic devices [30].
4) *ASTM E1250:* standard method for application of ionization chambers to assess the low-energy gamma component of ^{60}Co irradiators used in radiation hardness testing of silicon electronic devices [31].
5) *ISO/ASTM 51275*[1]: standard practice for use of a radiochromic film dosimetry system [96].

Test method 1019.9 specifies the dose rates required for doing TID testing to take into account effects such as "rebound." Although test method 1019.9 only applies to gamma ray testing, it can, nevertheless, be used as a guide for selecting the proton flux (dose rate) when doing TID testing with protons.

V. Radiation Test Facilities for TID Testing

A. Gamma Rays

The most commonly used source for simulation of ionization effects in silicon components (or materials) is ^{60}Co, which emits photons at two different energies (1.173 and 1.332 MeV), and has a half-life of 5.27 years. It is utilized for industrial irradiation, sterilization, radiotherapy, and biological research; gamma irradiators are, therefore, widely distributed geographically (Section V-E). Several standard commercial irradiation cells are on the market and contract irradiation facilities are often available. In these last years, ^{137}Cs (photon energy 0.662 MeV) is gaining increased acceptance, owing to its 30 years half-life and less severe shield requirements.

^{60}Co is produced from inactive ^{59}Co by heavy neutron irradiation in a nuclear reactor, while ^{137}Cs is formed as one of the most common fission products by the nuclear fission of ^{235}U and other fissionable isotopes in nuclear reactors.

A typical irradiator is a cylinder of ^{60}Co sealed in a steel jacket and placed in a thick lead shield or concrete cell, as shown in Fig. 26. A large number of electronic samples, arrayed in sockets in circuit boards, can be placed near the source and their response to the radiation can be monitored continuously via electrical connections. A source of medium strength has an activity of about tens of TBq; however, very large activities up to several PBq (10^{15} Bq) can be used in these irradiators leading to dose rates of several tens of kGy/h [97].

In some other commercial irradiators (called self-contained) the whole exposure takes place in an enclosed structure that can stand free in the corner of the laboratory as shown in Fig. 27 [99]. Because γ-rays are so penetrating, circuit boards can be stacked. In self-contained irradiators, large activities of up to 500 TBq of ^{60}Co and 750 TBq of ^{137}Cs can be used.

B. X-Rays

Being similar to γ-rays, X-rays induce ionization in materials. Even low-energy X-rays, provided they can be introduced into the active region of the device and the doses correctly estimated, can be an effective source of ionization. X-rays are generated when a beam of electrons bombards a target, usually of a high-Z metal, such as tungsten or copper. For high beam currents, the target must be cooled and the power supply large. The electron beam, colliding with the target, excites a "white spectrum" of bremsstrahlung X-rays (peaked broadly at about half the beam energy), upon which the K and L peak emissions of the target metal are superimposed (Fig. 1).

For tungsten, the main peak is at 59.3 keV (K line) and for copper at 8.04 keV (K line). The L line for tungsten is at 8.396 keV. It is normally desirable to filter these out, as well as lower energy white radiation, to avoid too much influence of the encapsulation on the dose penetrating to the active silicon device. Al and Be are typically used as filtering materials.

Fig. 26. Panoramic irradiator [98].

Fig. 27. Self-contained irradiation cell [100].

[1]This method replaces the Standard Practice ASTM E1275 withdrawn in 2002.

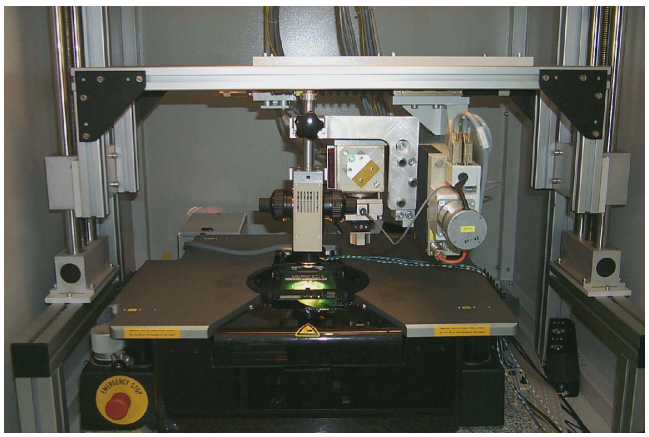

Fig. 28. X-ray tester at CERN. Seifert tube equipped with a semiautomatic wafer prober (Karl Suss PA200) mounting a thermal chuck of 8 in.

The use of X-rays requires care, but can be recommended for identification of sensitive technologies and the irradiation of limited number of devices. The main advantages are the low cost, the wide distribution of X-ray equipment, and the high safety standards available in such equipment. The care which is required involves the accurate administration of dose. In order to produce repeatable penetration power in an X-ray beam, the power-supply voltage and tube current must be stable. The degree of filtration must be kept constant, because this controls the X-ray photon energy spectrum. Both the degree of package penetration and the response of dosimetry are very sensitive to changes in energy spectrum (Fig. 1).

The use of low-energy (near 10 keV) X-ray testers for total-dose testing at wafer level [101] has become widely accepted where TID values are in the 10–100 kGy range and samples are small (see Fig. 28) [15]. This uses the tungsten L line as a collimated source fitted with a shutter and incorporated into a wafer prober. Surface dose rates of 0.5–2 kGy(Si)/min are achievable with this system. According to [101], more than 80% of the absorbed dose in silicon devices results from the tungsten L-line radiation. This allows the irradiation of a single selected die on a semiconductor wafer.

Flash X-ray generators are high-voltage machines that typically emit a very short (20–150 ns) pulse of very intense bremsstrahlung and X-rays. Because the ionizing dose per pulse is normally small, flash X-ray generators are usually not used to investigate TID-dependent phenomena. Therefore, their use in MOS device testing is normally restricted to the investigation of time-dependent effects, such as holes generation and charge transfer in gate insulators [1]. More information about the operation of a typical flash X-ray facility can be found in [102].

Dosimetry in X-rays facilities can be complex: the recommendations and procedures contained in the ASTM standards [49], [103] can be conveniently followed to organize dosimetry measurements in these facilities.

C. Electrons

All electron beams act as a source of ionization, but only the high-energy machines ($E \gg 0.1$ MeV) will also produce DD in semiconductors. Consequently, one of the most used sources of electrons is the Van de Graaff generator.

Fig. 29. RADEF linear electron accelerator on the right-hand side [104].

Van de Graaff generators can be designed to operate at any particle energy between 0.1 and 10 MeV. An electron beam is accelerated by the field between earth (the target) and an electrode charged to a very high-static potential. The charging is accomplished by means of a moving belt, which carries charge from a dc generator to the insulated "head" electrode. Potentials of 10 MV can be produced, but with more common machines 1 MV is the limit. Electrons released in the head are accelerated away from it, down to a vacuum pipe and emerge through a vacuum window in a beam of typically 20-mm diameter.

At 1 MeV, the electrons can travel several centimeters in air without great energy loss (Fig. 4), so that device irradiations can be performed in air. Typical device encapsulation (e.g., 0.3-mm Kovar IC lids) extracts energy and scatters 1-MeV electrons heavily. Therefore, there is always uncertainty about the dose received at the chip of an encapsulated device. The dose rate can be varied by altering beam current and beam focus, or sweeping the beam. Beam current can often be varied from 10 nA to 10 pA, which (in a 20-mm diameter beam) yields particle fluxes from about 2×10^{10} to 2×10^{13} e/cm^2/s. These fluxes correspond to dose rates from about 6 to 6 kGy/s.

LINACs provide intense pulses of electrons of higher energies, typically 4–40 MeV in rapid, square pulses. Electrons fired from an electron gun in a waveguide pickup RF energy and are accelerated from a few keV to several MeV. These accelerators are the one usually employed for medical treatments (see Fig. 29): average currents are again the microampere range, but instantaneous dose rates can be as high as 100 MGy/s.

During operation, in particular when the electrons are collided with a heavy metal target producing X-rays in the MeV range, LINACs may also generate a certain amount of "photo-neutrons" with a kinetic energy of a few MeV, which eventually reach thermal equilibrium within the LINAC room. This has to be accounted during TID testing when using neutron-sensitive devices. Usually there is, however, negligible risk from neutron activation [105].

D. Protons

Proton beams are mainly used for testing DD into encapsulated silicon components; however, they can also be interesting for TID testing (Sections I and III-G). The range in Si of a 15-MeV proton is ∼1.5 mm [19].

For the acceleration of protons to energies above 15 MeV, the most common machine is the cyclotron [106]. In this accelerator, high-frequency currents applied to two D-shaped electromagnets supply energy to a beam of hydrogen ions injected into a circular path. The trajectory of the particles is an outward spiral and particles can be picked off at an exit tube and transported till the test station [107]. A typical energy range for a cyclotron would be 20–600 MeV and fluxes of the order of 1×10^{13} p/cm^2/h are achieved. As the damage efficiency of protons in silicon falls off with increasing energy, 20 MeV is suitable also for TID testing. Since typical proton fluence levels ($E > 15$ MeV) for scientific space missions are at most 10^{11} p/cm^2, the fluence required for testing can be reached on a cyclotron in a fraction of an hour [108].

Some Van de Graaff machines can be converted for accelerating protons by reversing polarity and suppling a source of ionized hydrogen at the head. Other sources of high-energy protons are occasionally available for irradiation such as Pelletron generators [109] or proton LINACs, operating in the 10–100-MeV range that are used as injectors for GeV research accelerators (synchrotrons) and often preferred for proton testing in the HEP community [110].

The type of beam monitoring devices suitable for particle beam characterization and TID measurements in these types of facilities are summarized in Section III-G.

E. Radiation Test Facilities for TID and CERN Database

A list of gamma irradiation facilities, commonly used for qualifying components against TID effects, are listed in [111].

Several other facilities in Europe and around the world exist to perform TID (but also DD and SEE) radiation tests, as well as for radiation hardness studies. In order to fulfill the needs of the CERN community for searching irradiation facility infrastructures providing complementary and/or alternative conditions for radiation tests, a new irradiations facilities database was recently developed at CERN in the framework of the EU-funded AIDA-2020 project [112].

This database (www.cern.ch/irradiation-facilities) lists about 200 facilities (end of 2017). The initial set of data for this collection have been found in existent websites, as well as in other data collections such as the one published in occasion of the previous RADECS conferences [113]. In the database the users can search an irradiation facility by country, source, or radiation field and it includes information about the contact person, the institute, the facility, the irradiation conditions, as well as about safety and accessibility. The published data are open, but only the facility coordinators can edit the entries of their facilities or enter new facility information. The main advantage of this database, with respect to paper data collections or outdated static webpages [114], is the validity of the published data which is guaranteed by sending annual automatic update requests to the facility coordinators.

Fig. 30. IRRAD facility at CERN.

The database also gives information about the irradiation facilities operational at CERN [115] some of which, relevant for TID testing, are detailed in Sections V-E1 and V-E2.

1) CERN Proton Irradiation Facility (IRRAD): The main purpose of the IRRAD facility, located in the East Area of the proton synchrotron (PS) accelerator, is the qualification of components and particle detectors for the CERN HEP experiments (in particular trackers and calorimeters) [116]. The PS delivers to IRRAD a proton beam of 24 GeV/c, with a typical size of 12×12 mm^2 in spills, every 10 s on average. In this beam, samples up to 10×10 cm^2 in size can be exposed to a fluence of up to several 10^{15} p/cm^2. Smaller objects can be irradiated up to a particle fluence of 10^{17} p/cm^2. Irradiation experiments with a defocused proton beam or with larger objects are also possible. Furthermore, irradiation experiments at low temperature (−25 °C) or in cryogenic conditions (1.9 K) can be performed.

Concerning the samples, these can be placed on remotely controlled tables that can be moved along the x-axis, y-axis, and rotate around the beam axis, as shown in Fig. 30.

In addition, a shuttle system is available for the irradiation of smaller samples with maximum dimensions of 5×5 cm^2. This irradiation system can be moved from the outside area to the irradiation position, without the need to stop the proton beam. In order to align the beam properly, a dedicated beam profile monitor device [117] is used to provide a real-time display of the Gaussian beam profile. Moreover, dedicated software interfaces are used to control and monitor the IRRAD facility operation [118].

2) CERN Gamma Irradiation Facility (GIF++): GIF++ is mainly used to test gas detectors for the muon systems of HEP experiments. The GIF++ irradiation bunker, shown in Fig. 31, is located on the H4 beam line of the SPS North experimental area and combines a high-energy charged particle beam (muons up to 100 GeV) with a 0.66-MeV γ -rays background from a 14 TBq ^{137}Cs source (nominal activity).

Two large radiation fields (±37° degrees horizontally and vertically) allow testing detectors with sizes of up to several m^2, as well as a broad range of smaller prototype

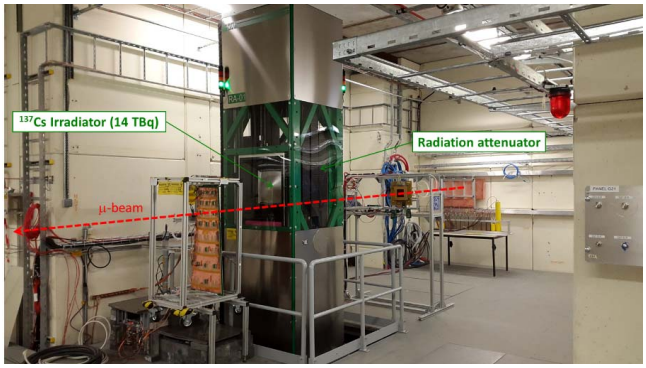

Fig. 31. GIF++ facility at CERN.

detectors, materials, and electronic components at a maximum dose rate of ∼2.5 Gy/h at a distance of 0.5 m from the source.

The photon flux of each irradiation zone is corrected by a lens to give equal counting rates over large planar detectors and can be tuned using a set of lead filters with attenuation factors up to about 50 000 [119]. This facility includes infrastructures as electronic racks, gas systems, radiation and environmental monitoring systems, beam- and cosmic-trigger chambers, and a dedicated area for the experiments preparation [120].

3) High-Energy Electrons (VESPER): Very energetic electron facility for space planetary exploration missions in harsh radiative environments (VESPER) is a high-energy electron beamline located in the CTF3 facility at CERN and used for radiation testing and characterization of electronic components for the operation in Jovian environment, as well as for the characterization of devices and detectors in a purely electromagnetic beam for high-energy accelerator applications [121].

VESPER uses a 200-MeV pulsed electron beam with an average flux of 10^8 e/cm^2/s. Copper blocks can also be remotely placed in the beamline in order to allow the progressive conversion of the electron beam into a bremsstrahlung photon beam.

4) ^{60}Co Facility (CC60): The CC60 facility, which is located in the same building as the new CERN radiation protection calibration facility (CALLAB) [122], is used for the qualification of the electronic components against TID effects. The facility exploits a 10 TBq ^{60}Co source (nominal activity) that can provide low and high dose rates, depending on the attenuators. For large systems, the total dose can reach from 1 to 10 kGy, whereas for smaller samples it can reach up to 100 kGy.

F. Practical and Safety Aspects of Radiation Tests

This section aims to give the reader some practical information that should be kept in mind while organizing a radiation test campaign for TID testing of electronics components, as well while planning the dosimetry measurements associated with it. The list below has been compiled after [5], [7], [9], and [111], as well as considering the feedback from various irradiation experiments and dosimetric measurements performed by CERN users supported by the author and his team.

1) Before Going to/at the Irradiation Facility:

1) Ensure that the facility is compliant with your requirements (energy, flux, etc.).
2) Ensure that your test system is compliant with the facility requirements (dimension, safety, etc.).
3) Ensure that a comprehensive test plan is in place and inform the facility about it. Test plans shall include all information necessary to ensure a successful radiation test campaign and as a minimum shall.
   a) Identify the irradiation source.
   b) Define dose rate, TID, and particle fluence steps.
   c) Identify the test samples (labeling) and lot number.
   d) Identify the parameters to be tested (and test standard employed, if any).
   e) Identify pass/fail criteria.
   f) Define a measurement sequence including timing requirements (e.g., time between testing and initiation of radiation tests).
   g) Define the test environment (thermal, etc.) and operational conditions.
   h) Define the annealing sequence.
4) Carry over spare devices in case retest is needed.
5) Inform the facility about the need of carry out post-irradiation (annealing) measurements.
6) Respect instructions of the facility about positioning and alignment of your samples. Get this checked by the facility staff before going, if possible.
7) Dosimetry is usually (but not always) done by facility staff. When this is available, it is likely to be accurate from ±5% to ±10%. Dosimetry may be complex and human errors can occur!
8) Possibly bring your own reference dosimeter. This is even more important when the experimental team is not present during irradiation.
9) Plan for test-samples transportation.
   a) It may be better to perform intermediate measurements at your laboratory and require shipping devices back and forth to the irradiation facility.
   b) Be aware of annealing during transportation (a cold shipping can be an option to mitigate).
10) Remember that personnel dosimetry is always required in facilities working with ionizing radiation. This may require paperwork to be provided in advance: medical certificate, radiation passport, etc. Sometimes, you may be required to carry with you also the personal dosimeter of your own home institution.

2) TID Test Organization in Proton Beams: Proton (and electron with $E > 10$ MeV) beams present the main problem of induced radioactivity. This increases with increasing energy of the particles. For this type of TID tests, care must be taken to follow the points in the following (in addition to those mentioned in Section V-F1).

1) Minimize the induced material activation from the conception of the radiation test: avoid using heavy metals in test fixtures. Al is often the material of choice because of its short-lived radioisotopes (e.g., ^{24}Na) that disappear

after about 1 week from the irradiation, thus reducing the radiation dose during manipulation.

2) Proceed with increasing TID steps, if possible (to minimize the amount of produced radioactive material, most likely to become a radioactive waste).
3) Foresee the adequate time slot for the radiation protection checks at the end of the test.
4) On-site transport of irradiated material must follow dedicated procedures established in the host irradiation facility/organization.
5) Shipping must follow the international regulations for transport of dangerous goods (e.g., ADR in case of road transport [123]). This requires additional time for the following:
   a) performing the radiological characterization of the material before shipping;
   b) preparing some mandatory paperwork from both sender and recipient side.

ACKNOWLEDGMENT

The author would like to thank the RADECS 2017 conference and short course organizers for the opportunity to present the work which is at the basis of this manuscript. He would also like to thank the fellow lecturers for the very helpful comments and inspiring advices, as well as F. Faccio, B. Gkotse, M. Glaser, G. Gorine, I. Mateu, M. Moll, and G. Pezzullo from CERN, Geneva, Switzerland, for their support and useful discussions and D. Wasek for her support in the preparation of this paper and for its careful review.

REFERENCES

[1] P. V. Dressendorfer and T. P. Ma, Eds., *Ionizing Radiation Effects in MOS Devices and Circuits*. New York, NY, USA: Wiley, 1989.

[2] A. Holmes-Siedle and L. Adams, *Handbook of Radiation Effects* (Oxford Science Publications), 2nd ed. London, U.K.: Oxford Univ. Press, 1993.

[3] *Standard Guide for Ionizing Radiation (Total Dose) Effects Testing of Semiconductor Devices*, Standard ASTM F1892-12, West Conshohocken, PA, USA, 2012.

[4] D. M. Fleetwood and H. A. Eisen, "Total-dose radiation hardness assurance," *IEEE Trans. Nucl. Sci.*, vol. 50, no. 3, pp. 552–564, Jun. 2003.

[5] S. Buchner, P. Marshall, S. Kniffin, and K. LaBel. *Proton Test Guideline Development—Lessons Learned*. Accessed: Oct. 2017. [Online]. Available: https://radhome.gsfc.nasa.gov/radhome/learned.htm

[6] A. Virtanen, "Facilities and radiation test methods," in *Proc. 10th Int. Workshop Radiat. Effects Semiconductor Devices Space Appl.*, 2013, pp. 90–95. [Online]. Available: https://eeepitnl.tksc.jaxa.jp/jp/event/RASEDA/index.html

[7] European Space Agency. (Jun. 2016). *ESCC Basic Specification No. 22900, Total Dose Steady-State Irradiation Test Method.* [Online]. Available: https://escies.org/

[8] *Test Method Standard Microcircuits*, Standard MIL-STD-883K, Department of Defense, 2017. [Online]. Available: https://landandmaritimeapps.dla.mil/Downloads/MilSpec/Docs/MIL-STD-883/std883mthd1000.pdf

[9] A. Zadeh, "Radiation hardness assurance & test facilities," presented at the 3rd Instrum. Workshop Eur. Jupiter Syst. Mission, Eur. Space Res. Technol. Centre, Noordwijk, Netherlands, Jan. 2010, pp. 1–27. [Online]. Available: http://sci.esa.int/jump.cfm?oid=46393

[10] S. Uznanski, B. Todd, A. Dinius, Q. King, and M. Brugger, "Radiation hardness assurance methodology of radiation tolerant power converter controls for large hadron collider," *IEEE Trans. Nucl. Sci.*, vol. 61, no. 6, pp. 3694–3700, Dec. 2014.

[11] *Standard Terminology Relating to Radiation Measurements and Dosimetry*, Standard ASTM E170-10, West Conshohocken, PA, USA, 2010.

[12] M. G. Stabin, *Radiation Protection and Dosimetry—An Introduction to Health Physics*. New York, NY, USA: Springer-Verlag, 2007.

[13] E. B. Podgorsak, *Radiation Oncology Physics: A Handbook for Teachers and Students*. Vienna, Austria: IAEA, 2005.

[14] K. Kerris, "Measurement and analysis of radiation effects in devices and ICS," in *Proc. NSREC*, New Orleans, LA, USA, Jul. 1992, pp. 1–50.

[15] *CERN EP-ESE, X-Ray Irradiation System*. Accessed: Oct. 2017. [Online]. Available: http://proj-xraymic.web.cern.ch/proj-XrayMIC/

[16] F. B. McLean and T. R. Oldham, "Basic mechanisms of radiation effects in electronic materials and devices," U.S. Army Lab Command, Harry Diamond Lab., Adelphi, MD, USA, Tech. Rep. HDL-TR-2129, 1987.

[17] E. Segre, Ed., *Experimental Nuclear Physics*, vol. 1. New York, NY, USA: Wiley, 1953.

[18] C. Patrignani *et al.*, "Review of particle physics," *Chin. Phys. C*, vol. 40, no. 10, p. 100001, 2016. [Online]. Available: http://pdg.lbl.gov/

[19] M. J. Berger, J. S. Coursey, M. A. Zucker, and J. Chang, "ESTAR, PSTAR, and ASTAR: Computer programs for calculating stopping-power and range tables for electrons, protons, and helium ions (version 1.2.3)," Nat. Inst. Standards Technol., Gaithersburg, MD, USA, Tech. Rep., 2005. Accessed: Oct. 2017. [Online]. Available: http://physics.nist.gov/Star

[20] M. J. Berger *et al.*, "Stopping powers for electrons and positrons," *Int. Commission Radiat. Units Meas.*,vol. 19, no. 2, Dec. 1984. [Online]. Available: https://doi.org/10.1093/jicru/os19.2.Report37

[21] J. H. Hubbell and S. M. Seltzer, "Tables of X-ray mass attenuation coefficients and mass energy-absorption coefficients (version 1.4)," Nat. Inst. Standards Technol., Gaithersburg, MD, USA, Tech. Rep., 2004. Accessed: Oct. 2017. [Online]. Available: http://physics.nist.gov/xaamdi

[22] A. H. Sullivan, *A Guide to Radiation and Radioactivity Levels Near High-Energy Particle Accelerators*. London, U.K.: Nuclear Technology Pub., 1992.

[23] T. E. Burlin, "Cavity Chamber Theory," in *Radiation Dosimetry*, vol. 1, F. H. Attix and W. C. Roesch, Eds., 2nd ed. Orlando, FL, USA: Academic, 1969, ch. 8.

[24] T. E. Burlin, "The theory of dosimeter response with particular reference to ionization chambers," in *Manual on Radiation Dosimetry*, N. W. Holm and R. J. Berry, Eds. New York, NY, USA: Dekker, 1970, ch. 2.

[25] *Standard Practice for Application of Thermoluminescence-Dosimetry (TLD) Systems for Determining Absorbed Dose in Radiation-Hardness Testing of Electronic Devices*, Standard ASTM E668-13, West Conshohocken, PA, USA, 2013.

[26] W. Buttler. Radiation Quantities and Units. Automation und Messtechnik GmbH (Automess). Accessed: Oct. 2017. [Online]. Available: http://www.automess.de/Messgroessen_E.htm

[27] M. M. Ninkovic, J. J. Raicevic, and F. Adrovic, "Air kerma rate constants for gamma emitters used most often in practice," *Radiat. Protection Dosimetry*, vol. 115, nos. 1–4, pp. 247–250, Dec. 2005.

[28] L. M. Unger and D. K. Trubey, *Specific Gamma Ray Dose Constants for Nuclides Important for Dosimetry and Radiological Assessment*, document ORNL/RSIC-45/R1, May 1982. [Online]. Available: https://www.orau.org/documents/ivhp/health-physics/ornl-rsic-45.pdf

[29] J. F. Ziegler and J. P. Biersack, "The stopping and range of ions in matter," in *Treatise on Heavy-Ion Science: Astrophysics, Chemistry, and Condensed Matter*, vol. 6, A. Bromley, Ed. New York, NY, USA: Springer-Verlag, 1985.

[30] *Standard Practice for Minimizing Dosimetry Errors in Radiation Hardness Testing of Silicon Electronic Devices Using Co-60 Sources*, Standard ASTM E1249-15, West Conshohocken, PA, USA, 2015.

[31] *Standard Test Method for Application of Ionization Chambers to Assess the Low Energy Gamma Component of Cobalt-60 Irradiators Used in Radiation-Hardness Testing of Silicon Electronic Devices*, Standard ASTM E1250-10, West Conshohocken, PA, USA, 2010.

[32] *Standard Practice for Use of a Polymethylmethacrylate Dosimetry System*, Standard ISO/ASTM51276, West Conshohocken, PA, USA, 2002.

[33] A. Micke, D. F. Lewis, and X. Yu, "Multichannel film dosimetry with nonuniformity correction," *Med. Phys.*, vol. 38, no. 5, pp. 2523–2534, May 2011.

[34] Ashland Advanced Materials, Niagara Falls, NY, USA. (2017). *Radiology Films*. [Online]. Available: www.gafchromic.com/gafchromic-film/radiology-films/index.asp

[35] Ashland Advanced Materials, Niagara Falls, NY, USA. (2017). *Radiotherapy Films*. [Online]. Available: www.gafchromic.com/gafchromic-film/radiotherapy-films/index.asp

[36] W. L. McLaughlin *et al.*, "Novel radiochromic films for clinical dosimetry," *Rad. Protection Dosimetry*, vol. 66, nos. 1–4, pp. 263–268, Jul. 1996.

[37] Far West Technology, Inc., Puyallup, WA, USA. (2017). *FWT-60 Series Radiachromic Dosimeters*. [Online]. Available: www.fwt.com/racm/fwt60ds.htm

[38] N. V. Klassen, L. van der Zwan, and J. Cygler, "GafChromic MD-55: Investigated as a precision dosimeter," *Med. Phys.*, vol. 24, no. 12, pp. 1924–1934, 1997.

[39] A. Niroomand-Rad *et al.*, "Radiochromic film dosimetry: Recommendations of AAPM radiation therapy committee task group 55," *Med. Phys.*, vol. 25, no. 11, pp. 2093–2115, Nov. 1998.

[40] *Standard Method for Calculation of Absorbed Dose From Gamma or X Radiation*, Standard ASTM E666-09, West Conshohocken, PA, USA, 2009.

[41] P. Bilski, "Lithium fluoride: From LiF:Mg,Ti to LiF:Mg,Cu,P," *Radiat. Protection Dosimetry*, vol. 100, nos. 1–4, pp. 199–205, 2002.

[42] C. Furetta, *Handbook of Thermoluminescence*, 1st ed. Singapore: World Scientific, 2003.

[43] F. Ravotti, "Development and characterisation of radiation monitoring sensors for the high energy physics experiments of the CERN LHC accelerator," Ph.D. dissertation, CERN, Univ. Montpellier, Montpellier, France, 2007, p. 241. [Online]. Available: https://cds.cern.ch/record/1014776

[44] B. Obryk, P. Bilski, and P. Olko, "Method of thermoluminescent measurement of radiation doses from micro gray up to a mega gray with a single LiF:Mg,Cu,P detector," *Radiat. Protection Dosimetry*, vol. 144, nos. 1–4, pp. 543–547, 2011, doi: https://doi.org/10.1093/rpd/ncq339

[45] D. Plattard *et al.*, "Characterization of an integrated sensor using optically stimulated luminescence for in-flight dosimetry," *IEEE Trans. Nucl. Sci.*, vol. 49, no. 6, pp. 1322–1326, Jun. 2002.

[46] W. Beezhold, D. E. Beutler, J. C. Garth, and P. J. Griffin, "A review of the 40-year history of the NSREC'S dosimetry and facilities session (1963-2003)," *IEEE Trans. Nucl. Sci.*, vol. 50, no. 3, pp. 635–652, Jun. 2003.

[47] L. Dusseau and J. Gasiot, "Online and realtime dosimetry using optically stimulated luminescence," *Int. J. High Speed Elect. Syst.*, vol. 14, no. 2, pp. 605–623, Jun. 2004.

[48] E. G. Yukihara, S. W. S. McKeever, and M. S. Akselrod, "State of art: Optically stimulated luminescence dosimetry—Frontiers of future research," *Radiat. Meas.*, vol. 71, pp. 15–24, Dec. 2014.

[49] *Standard Guide for Selecting Dosimetry Systems for Application in Pulsed X-Ray Sources*, Standard ASTM E1894-08, West Conshohocken, PA, USA, 2008.

[50] A. Holmes-Siedle, "The space-charge dosimeter: General principles of a new method of radiation detection," *Nucl. Instrum. Methods*, vol. 121, no. 1, pp. 169–179, Oct. 1974.

[51] A. Holmes-Siedle and L. Adams, "RADFET: A review of the use of metal-oxide-silicon devices as integrating dosimeters," *Int. J. Radiat. Appl. Instrum. C, Radiat. Phys. Chem.*, vol. 28, no. 2, pp. 235–244, 1986.

[52] A. G. Holmes-Siedle, F. Ravotti, and M. Glaser, "The dosimetric performance of RADFETs in radiation test beams," in *Proc. IEEE Radiat. Effects Data Workshop*, Honolulu, HI, USA, Jul. 2007, pp. 42–57.

[53] G. M. Mitev, S. Sarieva-Jordanova, and M. G. Mitev, "Enhanced readout system for RADFET dosimeters research," *Annu. J. Electron.*, pp. 250–253, 2015.

[54] L. Fröhlich and S. Grulja, "DOSFET-L02: An advanced online dosimetry system for RADFET sensors," in *Proc. IBIC*, Oxford, U.K., 2013, pp. 481–484, paper TUPC45.

[55] REM Oxford Ltd., Oxford, U.K.

[56] F. Ravotti, M. Glaser, A. B. Rosenfeld, M. L. F. Lerch, A. G. Holmes-Siedle, and G. Sarrabayrouse, "Radiation monitoring in mixed environments at CERN: From the IRRAD6 facility to the LHC Experiments," *IEEE Trans. Nucl. Sci.*, vol. 54, no. 4, pp. 1170–1177, Aug. 2007.

[57] M. S. Andjelković, G. S. Ristić, and A. B. Jakšić, "Using RADFET for the real-time measurement of gamma radiation dose rate," *Meas. Sci. Technol.*, vol. 26, no. 2, pp. 025004-1–025004-12, 2015, doi: 10.1088/0957-0233/26/2/025004.

[58] M. Soubra, J. Cygler, and G. Mackay, "Evaluation of a dual bias dual metal oxide-silicon semiconductor field effect transistor detector as radiation dosimeter," *Med. Phys.*, vol. 21, no. 4, pp. 567–572, Apr. 1994.

[59] R. B. Hayes, E. H. Haskell, A. Wieser, A. A. Romanyukha, B. L. Hardy, and J. K. Barrus, "Assessment of an alanine EPR dosimetry technique with enhanced precision and accuracy," *Nucl. Instrum. Methods Phys. Res. A, Accel. Spectrom. Detect. Assoc. Equip.*, vol. 440, no. 2, pp. 453–461, Feb. 2000.

[60] M. P. R. Waligórski, G. Danialy, K. S. Loh, and R. Katz, "The response of the alanine detector after charged-particle and neutron irradiations," *Int. J. Radiat. Appl. Instrum. A, Appl. Radiat. Isotopes*, vol. 40, nos. 10–12, pp. 923–933, 1989.

[61] W. L. McLaughlin and M. F. Desrosiers, "Dosimetry systems for radiation processing," *Radiat. Phys. Chem.*, vol. 46, nos. 4–6, pp. 1163–1174, Sep. 1995, doi: 10.1016/0969-806X(95)00349-3.

[62] E. Leon-Florián, H. Schönbacher, and M. Tavlet, *Data Compilation of Dosimetry Methods and Radiation Sources for Material Testing*, document CERN-TIS-CFM/IR/93-03, 1993.

[63] F. Coninckx, H. Schönbacher, M. Tavlet, G. Paic, and D. Razem, "Comparison of high-dose dosimetry systems for radiation damage studies in collider detectors and accelerators," *Nucl. Instrum. Methods Phys. Res. B, Beam Interact. Mater. At.*, vol. 83, nos. 1–2, pp. 181–188, Oct. 1993.

[64] M. Karacson, "Evaluation of the radiation environment of the LHCb experiment," Ph.D. dissertation, CERN, TU Wien, Vienna, Austria, 2016, p. 220. [Online]. Available: https://cds.cern.ch/record/2243499

[65] S. Beddar and L. Beaulieu, *Scintillation Dosimetry*, 1st ed. Boca Raton, FL, USA: CRC Press, 2016, p. 416.

[66] PTW-Freiburg. *MicroDiamond Detector Homepage*. [Online]. Available: http://www.ptw.de/micro_diamond.html

[67] M. A. McMahan *et al.*, "Standard practice for dosimetry of proton beams for use in radiation effects testing of electronics," in *Proc. IEEE Radiat. Effects Data Workshop*, Jul. 2008, pp. 135–141.

[68] G. F. Knoll, *Radiation Detection and Measurement*, 4th ed. Hoboken, NJ, USA: Wiley, 2011.

[69] K. Bernier *et al.*, "Calibration of secondary emission monitors of absolute proton beam intensity in the CERN SPS north area," CERN, Geneva, Switzerland, CERN Yellow Rep. 97-07, 1997, p. 22, doi: 10.5170/CERN-1997-007.

[70] C. M. Castaneda, "Crocker Nuclear Laboratory (CNL) radiation effects measurement and test facility," in *Proc. IEEE NSREC Radiat. Effects Data Workshop*, Jul. 2001, pp. 77–81.

[71] F. Ravotti *et al.*, "The beam profile monitoring system for the CERN IRRAD proton facility," in *Proc. Int. Beam Instrum. Conf.*, Barcelona, Spain, Sep. 2016, pp. 1–5, paper WEPG75.

[72] *CERN IRRAD Facility BPM Online Display*. Accessed: Oct. 2017. [Online]. Available: https://op-webtools.web.cern.ch/irrad/index.html

[73] K. M. Murray, W. J. Stapor, and C. Casteneda, "Calibrated charged particle radiation system with precision dosimetric measurement and control," *Nucl. Instrum. Methods Phys. Res. A, Accel. Spectrom. Detect. Assoc. Equip.*, vol. 281, no. 3, pp. 616–621, Sep. 1989.

[74] A. Dierlamm, "Studies on the radiation hardness of silicon sensors," Ph.D. dissertation, Inst. Experimentelle Teilchenphysik, Univ. Karlsruhe, Karlsruhe, Germany, Tech. Rep. IEKP-KA/2003-23, 2003.

[75] A. Curioni *et al.*, "Single- and multi-foils ^{27}Al(p,3pn)^{24}Na activation technique for monitoring the intensity of high-energy beams," *Nucl. Instrum. Methods Phys. Res. A, Accel. Spectrom. Detect. Assoc. Equip.*, vol. 858, pp. 101–105, Jun. 2017.

[76] S. Charalambus, J. Dutrannois, and K. Goebel, *Particle Flux Measurement With Activation Detectors*, document CERN DI/HP 90, Jul. 1966.

[77] V. Agoritsas, "Measurements of high-energy proton fluxes using foil activation techniques," Brookhaven Nat. Lab., New York, NY, USA, Tech. Note 135, 1977.

[78] *CERN Medipix Collaboration Webpage*. Accessed: Oct. 2017. [Online]. Available: http://medipix.web.cern.ch/

[79] M. Kroupa *et al.*, "A semiconductor radiation imaging pixel detector for space radiation dosimetry," *Life Sci. Space Res.*, vol. 6, pp. 69–78, Jul. 2015.

[80] E. H. M. Heijne and S. Pospíšil, "Method, apparatus and computer program for measuring the dose, dose rate or composition of radiation," U.S. Patent 8 168 953, May 1, 2012.

[81] N. Stoffle *et al.*, "Timepix-based radiation environment monitor measurements aboard the International Space Station," *Nucl. Instrum. Methods Phys. Res. A, Accel. Spectrom. Detect. Assoc. Equip.*, vol. 782, pp. 143–148, May 2015.

[82] L. S. Pinsky *et al.*, "Penetrating heavy ion charge and velocity discrimination with a TimePix-based Si detector (for space radiation applications)," *Nucl. Instrum. Methods Phys. Res. A, Accel. Spectrom. Detect. Assoc. Equip.*, vol. 633, pp. S190–S193, May 2011.

[83] M. Álvarez, C. Hernando, J. Cesari, A. Pineda, and E. Garcia-Moreno, "Total ionizing dose characterization of a prototype floating gate MOSFET dosimeter for space applications," *IEEE Trans. Nucl. Sci.*, vol. 60, no. 6, pp. 4281–4288, Dec. 2013.

[84] S. Danzeca *et al.*, "Characterization and modeling of a floating gate dosimeter with gamma and protons at various energies," *IEEE Trans. Nucl. Sci.*, vol. 61, no. 6, pp. 3451–3457, Dec. 2014.

[85] *Standard Practice for Use of an Alanine-EPR Dosimetry System*, Standard ISO/ASTM 51607, West Conshohocken, PA, USA, 2004.

[86] *Standard Guide for Selection and Calibration of Dosimetry Systems for Radiation Processing*, Standard ISO/ASTM51261, West Conshohocken, PA, USA, 2002.

[87] K. G. Kerris, "The theory and practice of radiation dosimetry in the radiation hardness testing of electronic devices and systems," U.S. Army Lab. Command, Adelphi, MD, USA, Tech. Rep. HDL-TR-2107, Apr. 1987.

[88] D. M. Long, D. G. Millward, R. L. Fitzwilson, and W. L. Chadsey, *Handbook for Dose Enhancement Effects in Electronic Devices*, document RADC-TR-83-84, Mar. 1983. [Online]. Available: http://www.dtic.mil/get-tr-doc/pdf?AD=ADA128490

[89] O. Oudea and R. Gaillard, "MEMSRAD: Final version of radiation requirements guidelines for MEMS devices," Astrium Space Transp., Paris, France, Tech. Note TN6, Nov. 2009. [Online]. Available: https://escies.org/download/webDocumentFile?id=58532

[90] S. Ibarmia *et al.*, "Experimental dose enhancement in multi-layer shielding structures exposed to high-energy electron environments," *IEEE Trans. Nucl. Sci.*, vol. 60, no. 4, pp. 2486–2493, Aug. 2013.

[91] B. Azais, P. Charre, C. Barillot, and O. Serres, "Updating the X-dose enhancement factor in recent technologies," in *Proc. Radiat. Effects Compon. Syst. Conf. (RADECS)*, Noordwijk, The Netherlands, Oct. 2004, pp. 579–586, paper ESA SP-536.

[92] J. R. Solin, "Electron collision dose enhancement," *IEEE Trans. Nucl. Sci.*, vol. 47, no. 6, pp. 2447–2450, Dec. 2000.

[93] M. Simons, R. L. Pease, D. M. Fleetwood, J. R. Schwank, and M. F. Krzesniak, "Dose enhancement in a room cobalt-60 source," *IEEE Trans. Nucl. Sci.*, vol. 44, no. 6, pp. 2052–2057, Dec. 1997.

[94] *Standard Guide for Estimating Uncertainties in Dosimetry for Radiation Processing*, Standard ISO/ASTM51707, West Conshohocken, PA, USA, 2005.

[95] European Space Agency. *ESA/SCC Basic Specifications*. Accessed: Oct. 2017. [Online]. Available: https://escies.org/

[96] *Standard Practice for Use of a Radiochromic Film Dosimetry System*, Standard ISO/ASTM 51275-13, West Conshohocken, PA, USA, 2013.

[97] *Manual on Panoramic Gamma Irradiators (Categories II and IV)*, document IAEA-PRSM-8 (Rev.1), IAEA, Vienna, Austria, 1996.

[98] Hopewell Designs Inc. [Online]. Available: http://www.hopewelldesigns.com

[99] *Manual on Self-Contained Gamma Irradiators (Categories I and III)*, document IAEA-PRSM-7 (Rev.1), IAEA, Vienna, Austria, 1996.

[100] NORDION, Gamma Technologies. [Online]. Available: http://www.nordion.com/gamma-technologies/

[101] L. J. Palkuti and J. J. LePage, "X-ray wafer probe for total dose testing," *IEEE Trans. Nucl. Sci.*, vol. NS-29, no. 6, pp. 1832–1837, Dec. 1982.

[102] R. B. Pietruszka, "Operation and characteristics of the flash X-ray generator at the Naval Postgraduate School," Ph.D. dissertation, Naval Postgraduate School, Monterey, CA, USA, 1989, p. 146. [Online]. Available: http://hdl.handle.net/10945/26130

[103] *Standard Guide for Use of an X-ray Tester (10keV Photons) in Ionizing Radiation Effects Testing of Semiconductor Devices and Microcircuits*, Standard ASTM F1467-11, West Conshohocken, PA, USA, 2011.

[104] Varian Clinac. [Online]. Available: https://www.varian.com/

[105] *Radiation Effects Facility RADEF*, Accelerator Lab., Univ. Jyväskylä, Jyväskylä, Finland. Accessed: May 2018. [Online]. Available: https://www.jyu.fi/science/en/physics/research/infrastructures/accelerator-laboratory/radiation-effects-facility

[106] M. Seidel and P. A. Schmelzbach, "Upgrade of the PSI cyclotron facility to 1.8 MW," in *Proc. 18th Int. Conf. Cyclotrons Appl.*, 2007, pp. 157–162. [Online]. Available: https://accelconf.web.cern.ch/accelconf/c07/

[107] *Proton Irradiation Facility PIF*, Paul Scherrer Inst., Villigen, Switzerland. Accessed: Oct. 2017. [Online]. Available: http://pif.web.psi.ch/

[108] W. Hajdas *et al.*, "Proton Irradiation Facility and space radiation monitoring at the Paul Scherrer Institute," *Phys. Med.*, vol. 17, no. 1, pp. 119–123, 2001.

[109] F. Hinterberger, "Electrostatic accelerators," in *Proc. CAS-CERN Accel. School KVI, Course Small Accelerators*, Zeegse, The Netherlands, May/Jun. 2005, pp. 95–112. [Online]. Available: https://cds.cern.ch/record/1005042, doi: 10.5170/CERN-2006-012.95.

[110] F. Ravotti, B. Gkotse, M. Glaser, P. Lima, E. Matli, and M. Moll, "A new high-intensity proton irradiation facility at the CERN PS east area," in *Proc. Int. Conf. Technol. Instrum. Particle Phys. (TIPP)*, Amsterdam, The Netherlands, Jun. 2014, p. 5, paper PoS(TIPP2014)354. [Online]. Available: https://pos.sissa.it/213/354/pdf, doi: https://doi.org/10.22323/1.213.0354

[111] M. Poizat, "Radiation environment and its effects in EEE components and hardness assurance for space applications," in *Proc. CERN-ESA-SSC Workshop*, Geneva, Switzerland, May 2017, pp. 1–4. [Online]. Available: https://indico.cern.ch/event/635099/

[112] *Advanced European Infrastructures for Detectors at Accelerators (AIDA-2020) Website*. Accessed: Oct. 2017. [Online]. Available: http://aida2020.web.cern.ch

[113] S. M. Barbero, S. K. Höffgen, G. Berger, and H. Guerrero, "Compendium of international irradiation facilities," in *Proc. RADECS*, Sevilla, Spain, 2011. [Online]. Available: http://www.radecs2015.org/compendium/

[114] B. Gkotse *et al.*, "IRRAD facility infrastructure upgrade," presented at the AIDA-2020 WP15 Meeting, Barcelona, Spain, 2017. [Online]. Available: https://indico.cern.ch/event/591285/

[115] B. Gkotse *et al.*, "Irradiation facilities at CERN," in *Proc. RADECS*, Geneva, Switzerland, to be published.

[116] F. Ravotti, B. Gkotse, M. Moll, and M. Glaser, "IRRAD: The new 24GeV/c proton irradiation facility at CERN," in *Proc. AccApp*, Washington, DC, USA, 2015, pp. 182–187. [Online]. Available: http://accapp15.org/

[117] B. Gkotse *et al.*, "The beam profile monitoring system for the IRRAD proton facility at the CERN PS east area," in *Proc. AccApp*, Washington, DC, USA, 2015, pp. 479–484. [Online]. Available: http://accapp15.org/

[118] B. Gkotse, M. Glaser, E. Matli, G. Pezzullo, and F. Ravotti, "Environmental monitoring, control and data management system of the CERN proton irradiation facility (IRRAD)," in *Proc. RADECS*, Geneva, Switzerland, to be published.

[119] D. Pfeiffer *et al.*, "The radiation field in the gamma irradiation facility GIF++ at CERN," *Nucl. Instrum. Methods Phys. Res. A, Accel. Spectrom. Detect. Assoc. Equip.*, vol. 866 pp. 91–103, Sep. 2017.

[120] M. R. Jaekel *et al.*, "CERN GIF++: A new irradiation facility to test large-area particle detectors for the HL-LHC program," in *Proc. Technol. Instrum. Particle Phys. Conf. (TIPP)*, Amsterdam, the Netherlands, Jun. 2014, p. 8, paper PoS(TIPP2014)102. [Online]. Available: https://pos.sissa.it/213/102/pdf, doi: https://doi.org/10.22323/1.213.0102

[121] M. Tali *et al.*, "High-energy electron-induced SEUs and Jovian environment impact," *IEEE Trans. Nucl. Sci.*, vol. 64, no. 8, pp. 2016–2022, Aug. 2017.

[122] M. Brugger, P. Carbonez, F. Pozzi, M. Silari, and H. Vincke, "New radiation protection calibration facility at CERN," *Radiat. Protection Dosimetry*, vol. 161, nos. 1–4, pp. 181–184, Oct. 2014.

[123] *The European Agreement concerning the International Carriage of Dangerous Goods by Road (ADR)*. Accessed: Oct. 2017. [Online]. Available: http://www.unece.org/index.php?id=43866&L=0